7-1-2014

Using Nd Isotopes to understand changes in continental weathering flux in Mid-Pennsylvanian (Desmoinesian) carbonate cycles

Phil Ragonese

Phil Ragonese

Candidate

Earth and Planetary Sciences

Department

This thesis is approved, and it is acceptable in quality and form for publication

Approved by the Thesis Committee:

Maya Elrick , Chairperson

Yemane Asmerom

Peter Fawcett

Using Nd Isotopes to understand changes in continental weathering flux in Mid-Pennsylvanian (Desmoinesian) carbonate cycles of the southwestern U.S.

By

Phil Ragonese

B.S. Geology, University of Wisconsin-Oshkosh, 2010

THESIS

Submitted in Partial Fulfillment of the
Requirements for the Degree of

Masters of Science

Earth and Planetary Sciences

The University of New Mexico
Albuquerque, New Mexico

July, 2014

Using Nd Isotopes to understand changes in continental weathering flux in Mid-Pennsylvanian (Desmoinesian) carbonate cycles.

By

Phil Ragonese

B.S. Geology, University of Wisconsin-Oshkosh, 2010
M.S. Earth and Planetary Sciences, University of New Mexico, 2014

ABSTRACT

Decades of study on Phanerozoic sedimentary deposits indicates that changes in Earth's orbital parameters are one of the main drivers of climate change on the 10^4-10^5 yr time scales, however understanding the relationships between climate change on coeval marine and continental deposits is difficult due to post-depositional erosion and tectonic processes. Nd isotopes measured in marine carbonates are a proxy for regional-scale continental weathering flux (CWF) and can help resolve these difficulties because its short residence time (less than ocean mixing times). This study focuses on cyclic Middle Pennsylvanian (Desmoinesian) marine successions from the Pedregosa (Arizona) and Bird Spring (southern Nevada) basin to address the interbasin and intrabasin response of Nd. Two types of orbital-scale subtidal cycles (1-7 m thick) are observed. Transgressive-regressive (TR) cycles (44%) are characterized by basal transgressive shallow subtidal deposits, deep subtidal deposits and capped by shallow subtidal deposits. Regressive (R) cycles (56%) are composed of basal deep subtidal deposits capped by shallow subtidal deposits; approximately 55% of T-R and R cycle caps show evidence of subaerial exposure. Due to the interpreted large magnitude sea-level changes and the

position of study areas along the inner/middle platform, the cycles are dominated by highstand (or interglacial) deposition. Seventeen cycles were sampled (<0.5 m sample resolution) for Nd-isotope analysis of whole rock limestones. ε_{Nd} values for all three locations range between -12.3 to -5.95 and two contrasting orbital-scale ϵ_{Nd} trends are recognized. Trend 1 (30%) is characterized by low ϵ_{Nd} (high CWF) during sea-level highstands (interglacial stages) and trend 2 (45%) is defined by high ϵ_{Nd} (low CWF) during sea-level highstands (interglacial stages). The absence of fluvial deposits within either studied basin combined with previous reports of thick Pennsylvanian loess deposits throughout the U.S. Southwest suggests an eolian source for the observed CWF. If an eolian interpretation is correct and we utilize recent climate modeling results for the late Paleozoic from Horton et al. (2012), which incorporates glacial-interglacial pCO2 changes which influences the position of the intertropical convergence zone (ITCZ) and low-latitude precipitation changes, then cycles that record high CWF (low ϵ_{Nd}) during interglacials (trend 1) represents drier/more windy climates in upwind source areas, whereas low CWF (high ϵ_{Nd}) during interglacials (trend 2) implies wetter/less windy climates in upwind source areas. This study illustrates the use of Nd isotopes in marine carbonates as novel proxy for detecting orbital-scale CWF changes in ancient marine systems.

TABLE OF CONTENTS

LIST OF FIGURES

LIST OF TABLES

Introduction

Decades of study on Phanerozoic sedimentary deposits indicates that changes in Earth's orbital parameters (i.e. Milankovitch cycles) are one of the main drivers of climate change on the 10^4-10^5 yr time scales (Anderson 1982; Goldhammer, 1987; Fischer and Bottjer, 1991; Olson and Kent, 1999; Laurin et al., 2005). Extensive stratigraphic, chemostratigraphic, and biostratigraphic research has documented the existence of orbitally forced climate cycles in marine (Anderson, 1982; Goldhammer et al., 1987, Gale et al., 2002, Laurin et al., 2005) and continental deposits (Olson and Kent, 1999; Aziz et al., 2007). However, understanding the relationships between climate change on coeval marine and continental deposits is difficult due to removal of continental strata by erosion or tectonism and because age-diagnostic fossils which occur within marine deposits are absent from continental deposits and vice-versa.

Common geochemical proxies for continental weathering flux (CWF--a term to define continental weathering rates and/or transport of continental material into the marine environment) include Sr- and Nd-isotope ratios. Sr-isotope ratios have been used in determining changes continental weathering flux vs. MOR activity (Spooner, 1976), but due to its long residence time (several My), once in the marine environment, it is not useful for detecting orbital-scale changes (Banner, 2004). Nd, however has a much shorter residence time (< 1000 yrs), and is an ideal geochemical proxy for assessing regional variations in continental weathering flux at 10^4-10^5 yr time scales.

When examining oceanic sediments in the Bay of Bengal, Burton and Vance (2000), showed that Nd isotopes varied systematically with $\delta^{18}O$ values and attributed this to increased fluvial sediment flux into the Bay of Bengal during interglacial periods

and a decrease in fluvially derived sediment during glacials. Using this as an example Theiling et al. (2012) examined Middle Pennsylvanian carbonate cycles that have been interpreted to be formed in response to large magnitude climate changes in response to glacio-eustasy based off $\delta^{18}O$ values (Elrick and Scott, 2010). Theiling et al. (2012) found that Nd-isotopes systematically changed within each cycle consequently describing a new method for detecting changes in sediment flux in pre-Pliestocene basins on 10^4-10^5 yr time scales.

Burton and Vance (2000) examined the relationship between ϵ_{Nd} and $\delta^{18}O$ from foraminifera, over the last 150 ky from the Bay of Bengal. Their results indicate that interglacial periods record lower ϵ_{Nd} values and are interpreted to result from increased monsoon strength and associated increased continental weathering and/or flux of fluvial-derived sediment. During glacial periods, there is a shift to higher ϵ_{Nd} values, which are interpreted to be due to a decrease in monsoon strength and decreased continental weathering and/or less fluvial influx.

Theiling et al. (2012) examined Middle Pennsylvanian, subtidal cycles of central New Mexico (Gray Mesa Formation) and found similar ϵ_{Nd} trends as Burton and Vance (2000) where values were highest (less CWF) at the tops and bottoms of cycles and lowest (more CWF) in the middle. The lowest ϵ_{Nd} values coincide with interglacial stages and the highest values coincide with early interglacial (cycle base) and early glacial stages (cycle top). These trends are interpreted to be a result of increased CWF during sea-level highstands and interglacial stages. This is interpreted to be a result of wetter and/or warmer interglacials which maximize weathering rates and fluvial transport of weathered material.

This study examined Nd-isotope ratios in cyclic, Pennsylvanian marine carbonates to assess orbitally driven changes in continental weathering flux. We compare local (i.e. same basin) and regional Nd-isotope ratio trends in Middle Pennsylvanian (Desmoinesian/Moscovian), cyclic carbonates from coeval equatorial and subtropical paleolatitudes to build on previous studies in order to assess Nd trends and how they fluctuate on a regional and local scale.

In this paper we 1) describe orbital-scale subtidal carbonate cycles and associated high-resolution Nd-isotope trends from three paleotropical Middle Pennsylvanian locations, and 2) using Nd isotopes as a proxy for CWF, discuss the climatic implications of observed orbital-scale CWF variability.

Geologic Background

Tectonics

The late Paleozoic tectonic history of southern North America was dominated by the onset of a collision between the North American craton and a southern landmass (Kluth and Coney, 1981; Kues and Giles, 2004), and a single worldwide Panthalassa ocean. The Ouachita-Marathon orogeny formed a series of north-northwest trending intracratonic block uplifts and associated "yoked" basins (Kluth and Coney, 1981). These uplifts, collectively called the Ancestral Rocky Mountains, are thought to be related to previous zones of weaknesses within the Proterozoic bedrock associated with earlier tectonic activity (Kluth and Coney, 1981).

The Pedregosa Basin is one example of a yoked basin in southeastern Arizona that developed as the Ouachita-Marathon orogeny continued and moved westward (Kluth and Coney, 1981). The Keeler Basin in southeastern Nevada initially developed as a

foreland basin related to the Antler orogeny (Dickenson, 2006). The Antler orogeny ceased in the Late Mississippian but the basin continued to evolve (Kluth and Coney, 1981; Dickenson, 2006). During the Pennsylvanian, the Keeler Basin developed into a series of uplifts and basins that were either associated with the Ouachita-Marathon orogeny or post-orogenic evolution of the Antler orogeny (Dickenson, 2006).

Pennsylvanian

The Pennsylvanian is a well-studied icehouse time interval with large ice sheets located in the southern hemisphere (Wanless and Cannon, 1966; Veevers and Powell, 1987; Poulsen, 2007). Fluctuations in ice volume produced widespread orbital-scale marine cycles of known glacial-eustatic origin (Wanless and Shepard, 1936; Heckel, 1994; Rygel et al., 2008; Elrick and Scott, 2010). Elrick and Scott (2010) reported $\delta^{18}O$ variations across a single cycle of 1‰-3.9‰ indicate eustatic changes up to 120m, which implies large magnitude climate changes.

This study focuses specifically on Middle Pennsylvanian marine successions in the U.S. Southwest, which developed adjacent to Proterozoic uplifts with known and distinct ϵ_{Nd} values (Bennett and DePaolo, 1987), across a wide range of paleolatitudes (from present day southern Arizona and New Mexico to northern Nevada and Colorado). Also, facies changes and biostratigraphy of interpreted glacial-interglacial cycles are well documented during this time in this region (Ross and Sabins 1965; Cassity and Lengenheim, 1966).

Southeastern Arizona

During the Pennsylvanian, southeastern Arizona was situated within 5^0 of the paleoequator (Figure 1). The Horquilla Limestone (~1600m thick) was deposited in the

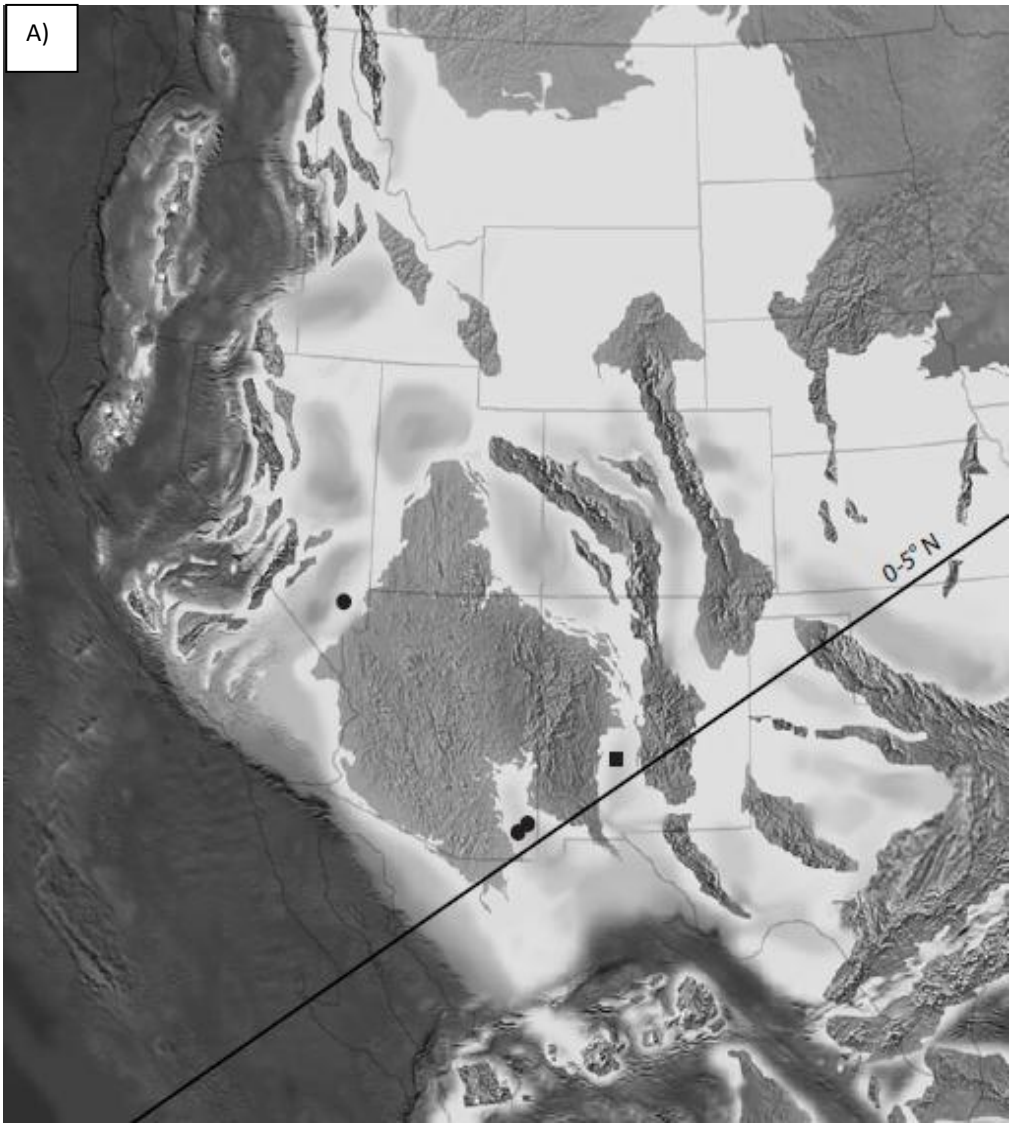
A)
0-5° N

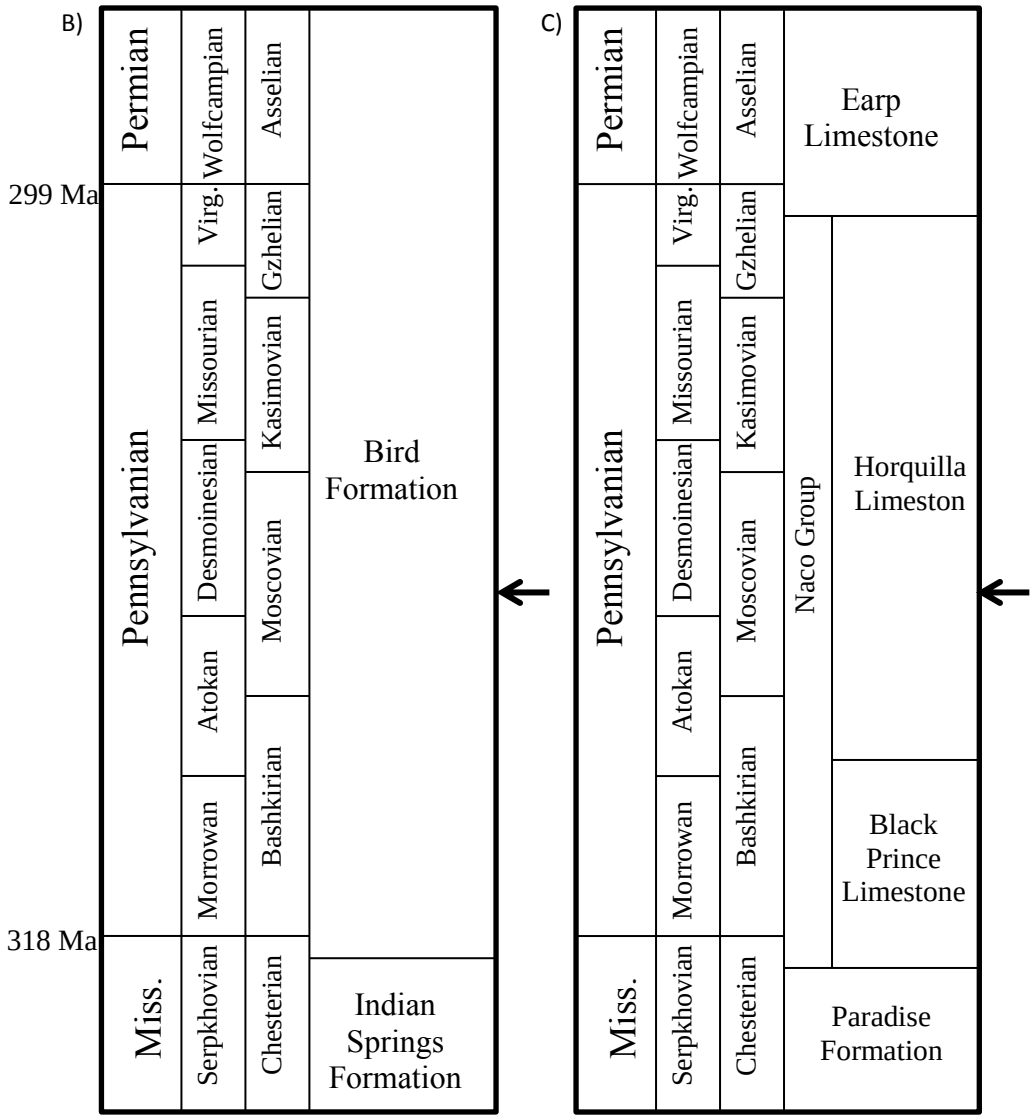
B)
299 Ma
318 Ma
Miss.
Serpkhovian
Chesterian
Pennsylvanian
Morrowan
Atokan
Desmoinesian
Missourian
Virg.
Bashkirian
Moscovian
Kasimovian
Gzhelian
Permian
Wolfcampian
Asselian
Bird Formation
Indian Springs Formation
C)
Miss.
Serpkhovian
Chesterian
Pennsylvanian
Morrowan
Atokan
Desmoinesian
Missourian
Virg.
Bashkirian
Moscovian
Kasimovian
Gzhelian
Permian
Wolfcampian
Asselian
Earp Limestone
Naco Group
Horquilla Limeston
Black Prince Limestone
Paradise Formation

Figure 1- A) Paleogeographic reconstruction of the western United States showing locations of Pennsylvanian uplifts as well as Pennsylvanian paleolatitudes. Black dots represent sections presented in this study and the black square is the location of results from Thieling, et al. (2012) (modified from http://www2.nau.edu/rcb7/garm310.jpg). B) Pennsylvanian chronostratigraphy for Arrow Canyon, Nevada and C) Pennsylvanian chronostratigraphy for Dry Canyon, Arizona and Gunnison Hills, Arizona. Arrows point towards the approximate location of sampled cycles.

Pedregosa basin and the age is constrained by fusulinid biostratigraphy (Ross and Sabins, 1965). This study concentrates on two locations with previously identified cycles, the Whetstone Mountains and western Gunnison Hills (Figure 1). At these locations Connolly and Stanton, (1992) identified ~40 meter-scale (shallowing upward) cycles within the Desmoinesian Horquilla Limestone.

Southern Nevada

Southern Nevada was situated approximately 15-20° N latitude during the Middle Pennsylvanian on the western edge of the Ancestral Rocky Mountains (Figure 1). The Arrow Canyon range provides excellent exposure of Mississippian through Late Pennsylvanian strata (Cassity and Langenheim, 1966; Bishop et al., 2010). The Bird Spring Formation (~750m thick) was deposited in the Keeler Basin from the Late Mississippian to Early Permain and whose age is constrained by fusulinid biostratigraphy (Cassity and Lengenheim, 1966).

Nd Systematics

^{143}Nd is the alpha decay product of ^{147}Sm, which has a half-life of 1.06 X 10^{11} years. Due to the difference in their ionic radii, during partial melting of the Earth's mantle, there is a slight fractionation, with Nd preferentially going into the melt, leaving the mantle depleted in Nd (i.e., Sm/Nd ratios are lower in the melt than in the depleted mantle). Similarly, fractional crystallization of the melt results in continental crust having lower Sm/Nd ratios than oceanic crust (Bennett and DePaolo, 1987). Due to these two episodes of fractionation, Nd- isotope ratios are different depending on the time at which the crust formed and the type of crust formed (Bennett and DePaolo, 1987).

Nd-isotope ratios are commonly reported as ϵ_{Nd} values given by the equation:

$$\epsilon_{Nd} = [(^{143}Nd/^{144}Nd)_{sample}/(^{143}Nd/^{144}Nd)_{CHUR}-1)* 10^4]$$

Where CHUR is the ratio of Nd within terrestrial chondritic material and provides an initial value of Sm/Nd that represents an undifferentiated mantle value at the time of interest.

Heterogeneity in ε_{Nd} is observed in modern ocean basins (Pacific, Indian, and Atlantic Oceans average $\varepsilon_{Nd(0)}$ are ~ -3, ~-8, and ~-12 respectively) and can be attributed to the average age of weathered material into the basins (Peipgras and Wasserburg, 1980). However, when calculating the residence time of Nd (τ_{Nd}) using total input from rivers, what was thought to be the dominant sources of Nd to the oceans (Goldstein et al., 1984), estimates range from 4,000 to 15,000 yrs (Johannesson and Burdige, 2007), exceeding the mixing time of the oceans. In order to elucidate this issue, known as the "Nd paradox," an additional and significant Nd source is required (Jeandel, et al., 1995; Arsouze et al., 2007; Johannesson and Burdige, 2007). Several models have been developed to account for the missing Nd including boundary exchange (Arsouze et al., 2007) and submarine groundwater discharge (Johannesson and Burdige, 2007; Johannesson et al., 2011).

Although modern studies do not attempt to examine Nd-isotpes ratios on the spatial resolution needed for comparison to our 2 Arizona sections, our results (Figure 2) suggest that the residence time of Nd within the Pedregosa basin is less than the mixing time of the basin. Taking into account the strong dependence of τ_{Nd} on basin volume (Johannesson and Burdige, 2007) combined with the (large) discrepancies in modern values (Johannesson and Burdige, 2007; Johannesson et al, 2011), this is assumed

reasonable, but cannot be precisely quantified for the time of deposition due to modern problems associated with the previously discussed "Nd paradox."

ϵ_{Nd} values of oceanic crust are high (enriched), and continental crust is commonly low (depleted) (Piepgras and Wasserburg, 1979; 1980). Due to these unique characteristics of Nd-isotope ratios can be used as a proxy for continental weathering flux. Nd-isotope ratios are an ideal proxy for determining continental weathering flux into the marine environment because, 1) the residence time of Nd in the ocean is <1000 years, which is less than the mixing time of the ocean and, therefore rapidly incorporated into coeval marine sediment (Tachikawa et al., 1999), 2) marine Nd is mainly controlled by continental flux (fluvial or other) into the marine environment (Goldstein and Jacobsen, 1987) and 3) Nd is diagenetically stable once incorporated into marine sediment (i.e., carbonates, phosphates, Fe-Mn crusts; Banner, 2004).

Methods

Samples for Nd analysis were collected from subtidal cycles of the Horquilla Limestone from the Whetstone Mountains and Gunnison Hills, southeastern Arizona and the Bird Spring Formation from the Arrow Canyon range, southern Nevada with a sampling resolution of every 30-50 cm. A total of 113 samples were collected for analysis from 3 non-coeval sections containing 4, 6, and 7 stacked cycles from Gunnison Hills, Dry Canyon, and Arrow Canyon respectively (Figure 2). To insure the validity of ϵ_{Nd} values we collected and compared whole rock ϵ_{Nd} values to 1) conodont apatite and 2) compared the same values from the same bed ~20 m apart along strike (Table 1). Also in order to assess whether or not we were obtaining Nd from carbonate (and not clays,

which would presumably contain a more continental Nd signal) we tested the same sample using different acids and acid strengths (Table 1).

.

Table 1- 143Nd/144Nd, apparent ε_{Nd} (value at present), Sm and Nd concentrations (ppm), ε_{Nd} (t=310 My) data for initial tests.

Sample #	$^{143}Nd/^{144}Nd$	Apparent εNd	Sm(ppm)	Nd(ppm)	εNd @ 310 My
DC 22.4 Conodont	0.51210616	-10.37	9.924	48.235	-7.52
DC 22.4 6N HCl	0.51192703	-13.87	0.240	1.261	-10.64
DC 22.4 1N HNO3	0.51193717	-13.67	0.331	1.738	-10.45
DC 22.4 1N HNO3 B	0.51193325	-13.75	0.308	1.571	-10.65
DC 22.4 Insoluble	0.51207380	-11.01	0.023	0.122	-7.64
DC 22.4 6N HCl- 2	0.51191270	-14.15	0.184	1.633	-9.07
DC 22.4 1N Acetic	0.51190957	-14.21	0.146	0.776	-10.94
DC 22.4 6N HCl A	0.51191728	-14.06	0.355	1.872	-10.82
DC 22.4 1N Ac A	0.51192502	-13.91	0.225	1.239	-10.47
DC 22.4 .5N Ac A	0.51192977	-13.82	0.224	1.223	-10.43
DC 22.4 .25N Ac A	0.51192907	-13.83	0.141	0.771	-10.41
DC 22.4 6N HCl B	0.51192462	-13.92	0.399	2.110	-10.66
DC 22.4 1N Ac B	0.51192409	-13.93	0.297	1.615	-10.55
DC 22.4 .5N Ac B	0.51192888	-13.83	0.279	1.510	-10.47
DC 22.4 .25N Ac B	0.51192584	-13.89	0.103	0.561	-10.50

Samples with an A are 20m away, along strike, from samples containing a B. t=310 My is assumed as an approximate age of deposition for cycles sampled in both the Horquilla Ls and Bird Spring Fm., in order to determine ε_{Nd} at the time of deposition.

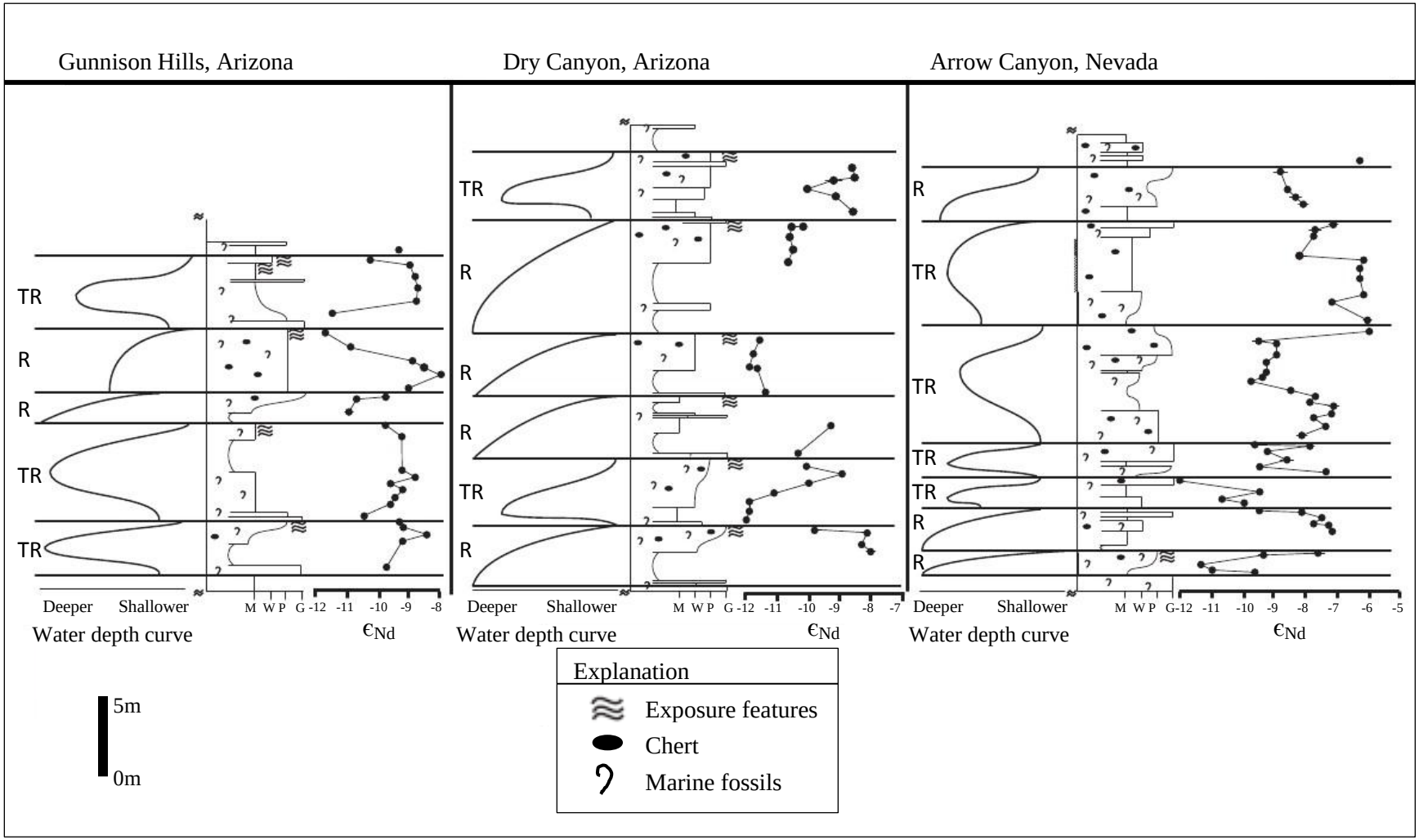

Figure 2- Cyclostratigraphy of the lower Desmoinesian Horquilla Limestone at Dry Canyon and Gunnison Hills and the Bird Spring Formation. At Arrow Canyon versus relative water depths determined from facies analysis and ε_{Nd} trends. T represents transgressive cycle types and TR represents transgressive-regressive cycle types.

Nd isotopic analyses were performed on crushed whole rock limestone (~250µg). Aside from the initial acid used for dissolving the carbonate (we use 0.5N Acetic acid vs 6N HCl) we will follow the methodology of Theiling et al. (2012). The crushed limestone was initially dissolved in 0.5N Acetic acid, which was set on a hot plate for 2.5 hrs. The soluble and insoluble fractions were then separated using a centrifuge. The soluble fraction was then dried down and dissolved in 7N HNO_3, which was successively dried and dissolved in 15N HNO_3. The dried sample was then dissolved in 2 mL of 1N HNO_3 followed by the addition of a calibrated spike with a known $^{147}Sm/^{150}Nd$. REE's were concentrated using standard resins (TRU-SP) and column work using a modified method of Asmerom (1999). Following separation of REE we concentrated the Sm and Nd using REE exchange columns using a modified method of Asmerom (1999). The Sm and Nd fractions were then dried down and dissolved in 1 mL of 3% HNO_3 and analyzed using a Thermo Neptune multi-collector inductively coupled plasma mass spectrometer (MC-ICPMS) located at the University of New Mexico Radiogenic Isotope Lab.

Lithofacies and Depositional environments

Three separate and non-coeval stratigraphic sections were measured and described using Dunham's classification and facies analyses (i.e., changes in grain size, sedimentary structures, fossils, etc.) which were used to interpret depositional environments as well as changes in relative sea level through time. A total of 8 facies were identified ranging from shallow to deep subtidal depositional environments (Table 2; 3).

Shallow subtidal facies

Shallow subtidal facies include crinoidal grainstone/packstone and skeletal packstone subfacies (Tables 2; 3). These facies are observed in 10 out of 12 cycles and occur at the tops or bases (i.e. regressive or transgressive) of most cycles. Diversity and abundance of biota suggests open marine conditions, while little to no muddy matrix indicates higher energy conditions.

(1) Skeletal grainstone subfacies represent deposition in a high energy, open marine environment. This is supported by abundance of abraded shells of open marine organisms (crinoids and brachiopods) and low mud content.

(2) Skeletal packstone subfacies were deposited in moderate energy and open marine conditions, as is evident by the abundance of open marine fauna (crinoids and brachiopods), low mud content and grain size (Wilson, 1975; Goldhammer et al., 19??; T.D. Olszewelski and M.E. Patzokowsky, 2003).

Intermediate subtidal

Intermediate subtidal facies include skeletal wackestone/packstone, argillaceous-skeletal wackestone/packstone, and nodular-bedded argillaceous skeletal wackestone subfacies (Tables 2; 3). These subfacies are most commonly found in the middle of cycles, but occasionally occur at cycle tops.

(3) Cherty-skeletal wackestone/packstone subfacies represent deposition in moderate energy with slightly restricted conditions. This is indicated by the low diversity of fauna; however a high abundance of skeletal fragments and common bioturbation suggests waters were (Elrick and Read, 1991; Soreghan and Giles, 1999; Scott and Elrick, 2004; Bishop et al., 2009).

(4) Skeletal wackestone/packstone subfacies represent deposition in moderate energy environments, due to the presence of abraded fenestrae bryozoan and moderate to high mud content, with normal marine conditions as evident by the high diversity and abundance of open-marine fauna (i.e. crinoids) (Algeo et al., 1991; Elrick and Read, 1991).

(5) Argillaceous skeletal wackestone/packstone subfacies were deposited in relatively low energy environments in partially stressed conditions (i.e. lack of light due to abundance of clays). The low diversity and relatively low abundance of fauna support this view (Algeo et al., 1991).

(6) Thin-bedded skeletal wackestone subfacies were deposited in relatively low to moderate energy environments. This is supported by the high amount of muddy matrix (Algeo et al., 1991).

Deep subtidal

Deep subtidal facies include lenticular skeletal wackestones, lime mudstone, and thin-bedded skeletal wackestone (Tables 2; 3). Deep subtidal facies are present in all cycles and subfacies represent the deepest water deposits and commonly occur at the bases and rarely in the middle of cycles.

(7) Lime mudstone subfacies represent deposition in low energy, low O_2 conditions. This is supported by the dark color, the lack of skeletal organisms, high mud content and abundant planar laminations and thin bedding indicating suspension settling (Algeo et al., 1991; Soreghan and Giles, 1999; Scott and Elrick, 2004)

(8) Lenticular skeletal wackestone subfacies are interpreted to be deposited in low energy and represent farthest reaching tongues of intermediate subtidal or storm deposits.

This is supported by their occurrence within the lime mudstone subfacies and lenticular geometry.

Exposure Features

Dark calcite-filled cracks

Description: Vertical to horizontal dark-calcite filled cracks are common features in the Horquilla Limestone and occur at the tops of many subtidal cycles. The abundance of dark calcite-filled cracks decreases downward and generally penetrates to depths of 1-2 meters. Dark-calcite filled cracks are stringy and irregular, but can occur as pebbles. Individual dark calcite-filled cracks pinch out at depth and laterally and bifurcate (Figure 3 A and B) and form crack patterns that include horizontal joint planes, curved planes and craze planes as described by Goldstein, 1988 (Figure 3 A and C).

Interpretation: The dark gray to black carbonate infilling cracks is interpreted as pedogenically precipitated calcite or calcrete. During sea-level fall and lowstand, subaerial exposure of subtidal deposits results in drying, which produced initial micro-fractures for meteoric waters to infiltrate, dissolve and create larger vertical and horizontal cracks. Plants begin to colonize and acidic micro environments due to root respiration aid in the dissolution of the host limestone where calcrete subsequently accumulates. Similar cycle–capping calcretes are described in Pennsylvanian strata of New Mexico (Goldstein, 1988b), and Arizona (Goldhammer and Elmore, 1984) and are attributed to subaerial exposure and pedogenesis. The dark color is most likely due to the preservation of organic matter (Strasser, 1984; Goldstein et al., 1991) and distributive bifurcation distinguishes root systems from animal burrows.

Table 2- Facies Description of the Horquilla Limestone

Facies name	Lithology	Unit thickness/Bedding characteristics	Skeletal components	Sedimentary /biological structures	Other	Cycle Position
Shallow subtidal						
Skeletal grainstone	crinoidal grainstone, fusulinid-skeletal grainstone	0.5m – 1.5m thick; Medium- to thick-bedded; gradational to sharp lower contact, sharp upper contact	Dominantly crinoid fragments and mollusk fragments, common rugose coral and fusulinids, rare colonial coral and chaetetes	Minor rip-up clasts Massive (bioturbation ?)	Common chert nodules (20-50cm)	Occur at cycle bases and/or at cycle tops
Skeletal packstone	Crinoid-brachiopod packstone, crinoid-fusulinid packstone,	<0.5m – 1m thick; Medium- to thick-bedded gradational to sharp upper and lower contacts	Abundant crinoid fragments, very common brachiopod fragments, common gastropods, rugose and fusulinids, rare colonial coral	None (bioturbation ?)	None	At or near cycles tops
Intermediate Subtidal						
Cherty skeletal wackestone/ packstone	Crinoid-brachiopod wackestone/ packstone	1m- 4m thick; Medium- to thick- bedded,	Abundunt crinoid and mollusk fragments	Common bioturbation	Abundant chert nodules (10-50cm)	Near middle of cycle
Argillaceous skeletal wackestone/ packstone	Fusulinid- fenestrae bryozoan wackestone/ packstone, crinoid-	0.5m -1.5m thick; Thin, nodular, bedding, ,	Abundant crinoid fragments and fusulinids, very common fenestrae	Common bioturbation	Clay seems (<1-3cm thick) laterally discontinuous,	Near middle of cycle

	brachiopod wackestone		bryozoan, common whole mollusks, rare colonial coral		common chert nodules (10-30cm)	
Thin-bedded skeletal wackestone	Crinoid-brachiopod wackestone	<0.5m- 1.5m thick; Thin nodular-bedded, , typically gradational upper contact	Abundant crinoid fragments, common brachiopod and bivalves, rare rugose	Mottled appearance (bioturbation ?)	Minor chert nodules (10cm-30cm)	At or near cycle base
Deep Subtidal						
Lime mudstone	Dark gray	<0.25cm - 1m; Thin nodular-bedded,	rare mollusk and crinoid fragments	Common planar laminations		Occur at or near cycle base

Table 3. Facies Description of the Bird Spring Formation

Facies name	Lithology	Unit thickness/Bedding characteristics	Skeletal components	Sedimentary structures	Other	Cycle Position
Shallow Subtidal						
Skeletal Grainstone	crinoidal grainstone, fusulinid skeletal grainstone	Medium- to thick-bedded (0.5m – 1.5m) ; gradational to sharp lower contact, sharp upper contact	Dominantly crinoid fragments and mollusk fragments, common rugose coral and fusulinids, rare colonial coral and chaetetes	Minor rip-up clasts	Common chert nodules (20-50cm)	Occur at cycle bases and/or at cycle tops
Intermediate subtidal						
Skeletal wackestone/ packstone	Crinoid-brachiopod wackestone/ packstone, crinoid-rugose wackestone/ packstone	Thin- to medium-bedded, nodular to planar bedding	Common crinoid fragments, rugose, mollusk fragments and fusulinids, rare colonial coral	None	Common chert nodules (10cm-30cm)	Occurs near the middle and top of cycles
Argillaceous skeletal wackestone/ packstone	Fusulinid-fenestrae bryozoan wackestone/ packstone, crinoid-brachiopod wackestone	Thin, nodular, bedding, 0.5m - 1.5m thick,	Abundant crinoid fragments and fusulinids, very common fenestrae bryozoan, common whole mollusks, rare colonial coral	Common bioturbation	Clay seems (<1-3cm thick) laterally discontinuous, common chert nodules (10-30cm)	Near middle of cycle
Deep subtidal						
Lime Mudstone	Skeletal lime mudstone, chert-clast lime	Thin nodular-bedded, <0.25cm - 1m	rare mollusk and crinoid fragments	Common to rare planar laminations		Occur at or near cycle base

	mudstone					
Lenticular skeletal wackestone	Crinoid-mollusk wackestone	Lenticular beds, <0.5 m thick	common crinoid and mollusk fragments	none		Occur at or near cycle base

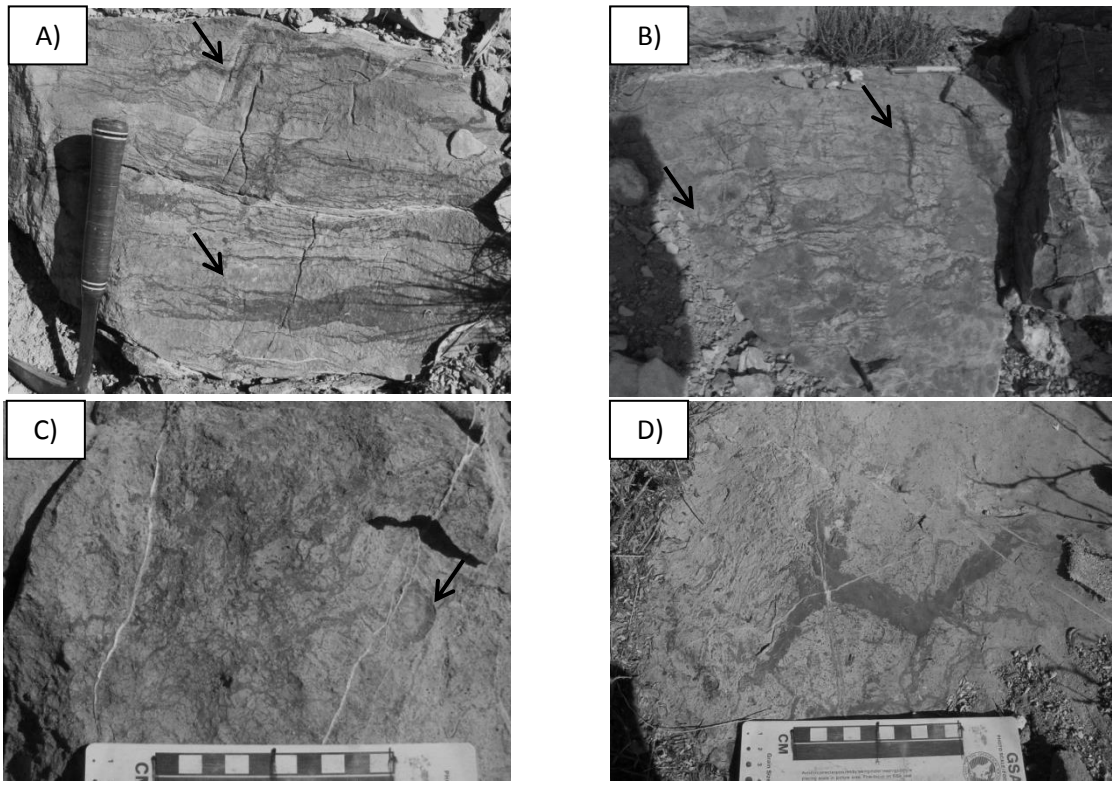

Figure 3- Field photographs of calcretes within the Horquilla Limestone. A) Arrows highlight the distributive nature of calcretes. Note how the calcrete branches outwards (horizontally) from a single vertical calcrete next to the top arrow. B) Desiccation crack patterns within the Horquilla Limestone. The top arrow is pointing at horizontal sheet cracks. The bottom arrow is showing craze planes or skew planes (again note the distributive nature of these calcretes and how horizontal calcretes appear to be branching out from vertical calcretes). C) The arrow is pointing towards curve planes and to the left of the arrow are craze planes, both of which are desiccation patterns commonly formed by pedogenesis. D) Bedding plane view of polygonal crack patterns associated with microkarst formation during subaerial exposure.

Dissolution Features

Description: Irregular dissolution surfaces occur at the tops of subtidal cycles and are sharp and undulating with 5- 20 cm of relief.

Interpretation: Dissolution surfaces are interpreted as microkarst features formed during sea-level falls and lowstands as undersaturated meteoric waters infiltrated fractures/joints/bedding planes dissolving pre-existing subtidal carbonates.

RESULTS AND INTERPRETATIONS

Cyclostratigraphy results

Two types of subtidal cycles (average thickness 4.1m) are observed. Transgressive-regressive (TR) cycles (45%) are characterized by a basal transgressive skeletal pack-grainstone (shallow subtidal), nodular- to thin-bedded argillaceous lime mudstone or covered intervals (deep subtidal), capped by skeletal pack-grainstone (shallow subtidal). Regressive (R) cycles (55%), are composed of basal nodular- to thin-bedded argillaceous lime mudstone (deep subtidal) or covered intervals capped by skeletal pack-grainstone (shallow subtidal) (Figure 4). Cycle boundaries are defined by 1) shallow subtidal facies directly overlain by deeper subtidal facies along a marine flooding surface or 2) subaerial exposure features overprinting subtidal facies. It is important to note that basal transgressive pack-grainstone (vs. cycle capping pack-grainstone) were identified mainly by the occurrence of subaerial exposure features developed within underlying subtidal facies.

The average duration for cycles within the Horquilla Limestone is 95 ka based on the ~3.7 My duration of the Middle Pennsylvanian (Desmoinesian/Moscovian; Gradstein et al., 2004) and the occurrence of ~39 Desmoinesian cycles occurring at the two Arizona

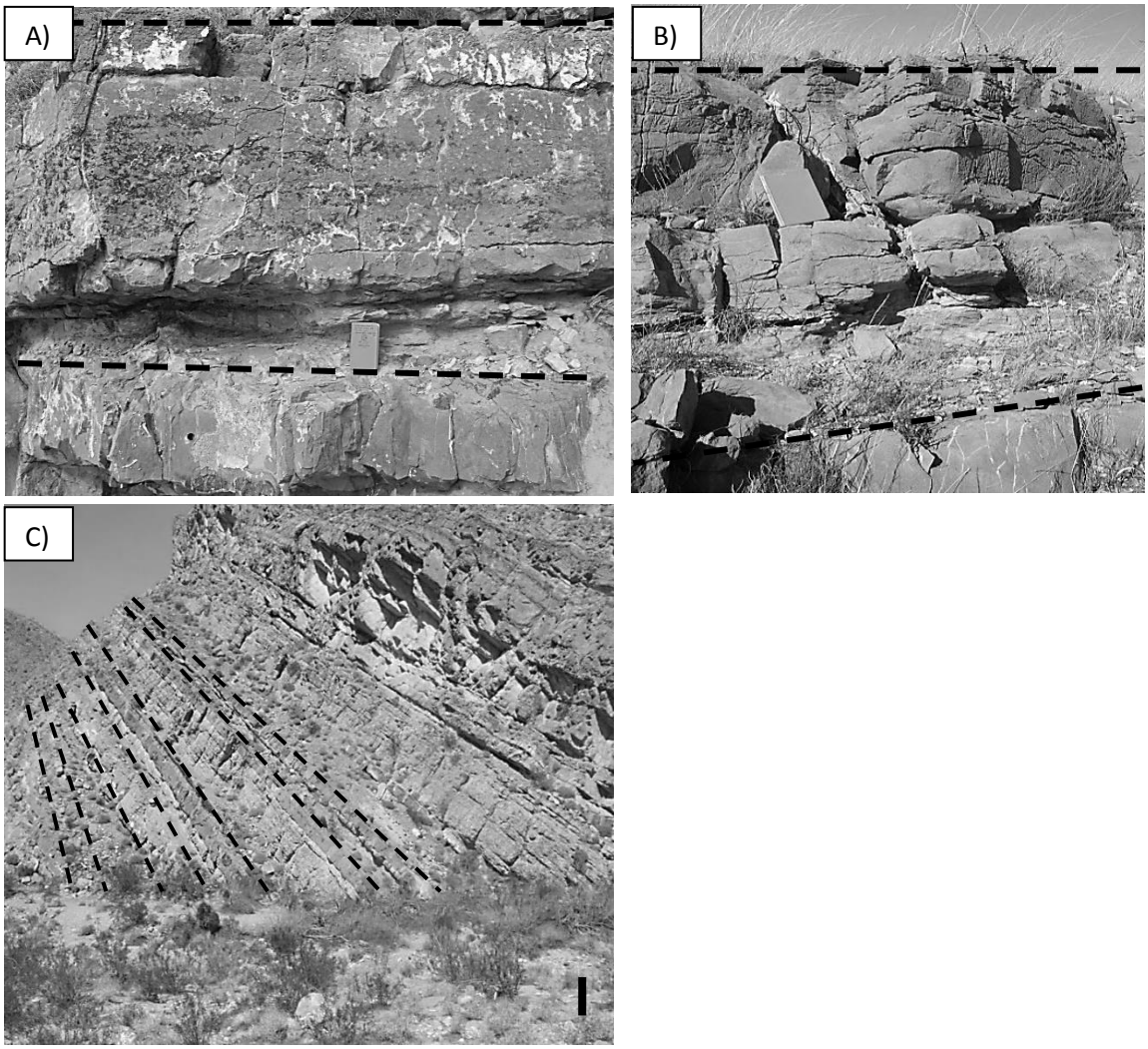

Figure 4- Field photographs of carbonate cycles where dashed lines indicate cycle boundaries. A) Shows a typical regressive cycle from Arrow Canyon, Nevada. B) Typical regressive cycle from Dry Canyon, Arizona. Both A) and B) have deep subtidal bases (Lime mudstone/lenticular skeletal wackestone) which are capped by shallow subtidal facies (Skeletal grainstone/packstone). C) Stacked cycles from Arrow Canyon, Nevada. The solid vertical line is ~2 m.

localities. Cycles in the Bird Spring Formation have estimated durations of ~100 ka based on the number of cycles identified by Bishop et al. (2010) who also use the time scale of Gradstein et al. (2004). Both estimates are consistent with short eccentricity periodicities.

Cyclostratigraphic interpretations

Two different mechanisms have been suggested as the cause(s) of subtidal cycle formation including glacio-eustasy and/or episodic tectonism.

High-frequency episodic tectonism has been cited as a cause for the development of carbonate cycles where accommodation spaced developed by fault-induced downdropping is progressively filled with upward-shallowing carbonates (Cisne, 1986; Hardie et al., 1986). In order to produce the succession of carbonate cycles observed at the 3 study areas, high-frequency downdropping of 2-10m would have had to occur throughout a >20 my time interval (Connolly and Stanton, 1992; Bishop et al., 2010). This scenario is problematic due to 1) no modern analogue of persistent and widespread downdropping on 10^4-10^5 yr time intervals has been reported, and 2) there is no evidence of repeated 10^4-10^5 yr faulting in the Southwest during this time interval (Kluth and Coney, 1981; Dickinson and Lawton, 2003)

High-frequency, large-amplitude (>50m), glacio-eustasy as the driver for repeated water depth changes is suggested by widespread correlation of individual cycles (Busch and Rollins, 1984; Connolly and Stanton, 1992; Ritter et al., 2002; Eros et al., 2011), juxtaposition of offshore through shoreface facies (Heckel, 1994), relief preserved on subaerial exposure paleosurfaces (Soreghan and Giles 1999) and $\delta^{18}O$ isotopic shifts

(Joachimski et al., 2006; Elrick and Scott, 2010; Theiling et al., 2012) and best explains the development of subtidal cycles described in this study.

TR and R cycles occur in all 3 sections. In Arizona most (91%) contain exposure features however, in Nevada no macroscopic evidence of subaerial exposure was identified, but Bishop et al. (2010) recognized microscopic features indicative of subaerial exposure including rhizoliths, meteoric cements, and moldic porosity developed within subtidal carbonates.

Due to the studied cycles developing in an updip position along the carbonate ramp, the subtidal cycles 1) record an abbreviated record of sea level rise and fall, but 2) do not record each sea level rise and fall (Figure 5). Subaerial exposure features (i.e. calcrete precipitated within extensive dissolution features) as well as regressive cycle types are evidence for an abbreviated record. This evidence along with interpreted high-amplitude Middle Pennsylvanian sea level changes suggest the studied areas do not record each sea level cycle with missed sea-level oscillations referred to as missed beats (Figure 5). Of the sea level oscillations that get recorded, only the late rise, highstand and earliest fall are recorded due to the interplay between sediment supply, sea level rise/fall rates, and subsidence. It is important to note that eustatic highstand is recorded within regressive facies in the middle or upper parts of cycles when sedimentation outpaced accommodation gains. The deepest water facies at the cycle base or mid cycle represent times of maximum rates of sea-level rise (Figure 6).

The interpreted sequence of events for the generation of a subtidal transgressive-regressive cycle would be as follows. During high-frequency late sea level rise (late

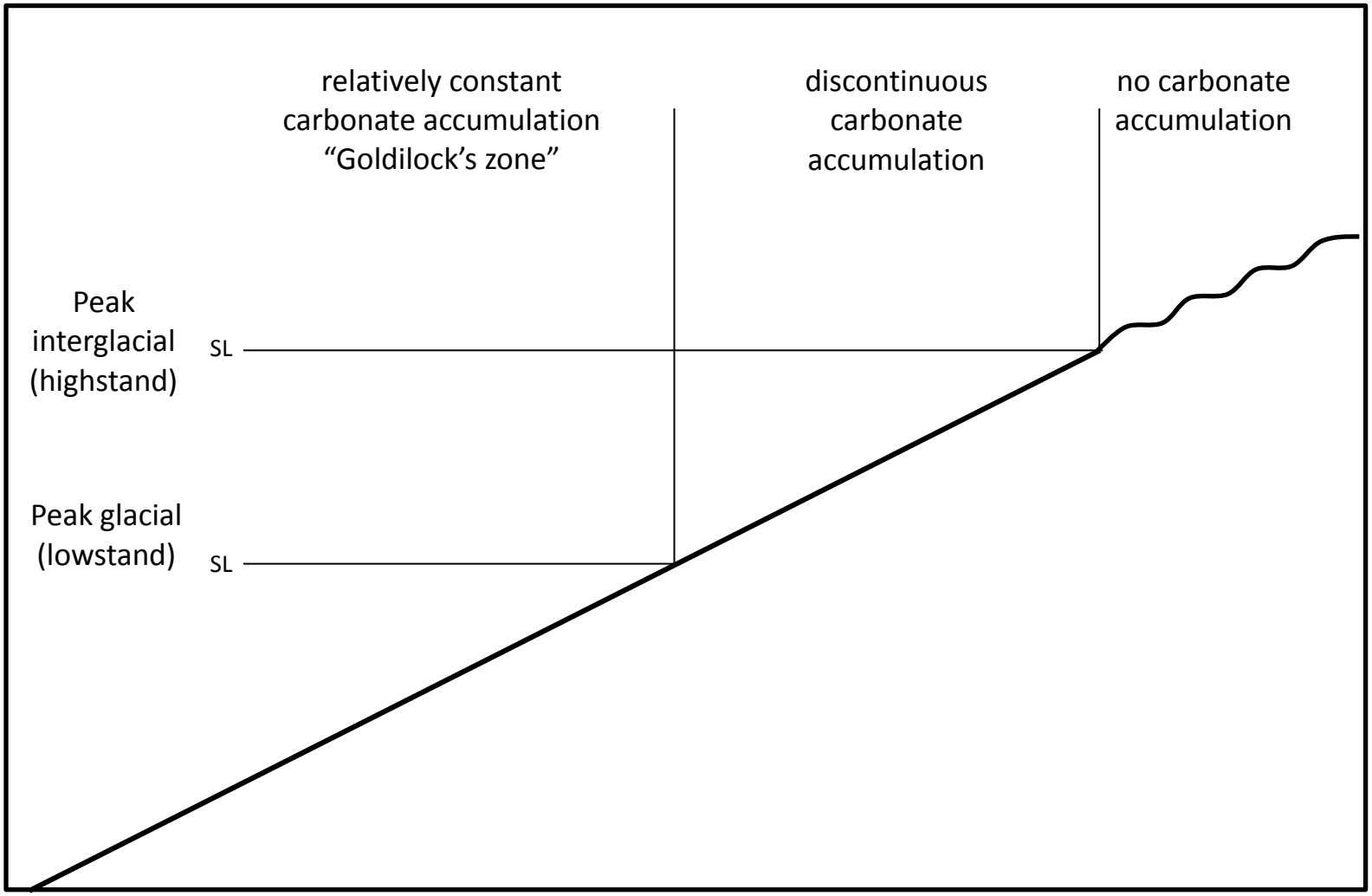
relatively constant
carbonate accumulation
"Goldilock's zone"
discontinuous
carbonate
accumulation
no carbonate
accumulation
Peak
interglacial
(highstand)
SL
Peak glacial
(lowstand)
SL

Figure 5- Simplified figure showing variation in carbonate accumulation based on position along a ramp. The sediment surface is represented by the thick black line. The thin black line represents sea level. The top set of lines represents sea level during peak interglacial periods (high sea level) and the bottom set of horizontal lines represent sea level during glacial periods (low sea level). Areas still submerged during peak glacial periods represent the Goldilocks zone, where accumulation would occur over all sea level cycles. The area exposed during peak interglacials is the position that would never accumulate carbonates and in between these extremes variable carbonate deposition occurs, where carbonates can accumulate for any fraction of sea level cycles. The number of wet-dry cycles associated with each carbonate accumulation zones is what would be expected if the results of Horton et al. (2012) are correct (refer to text discussion for more).

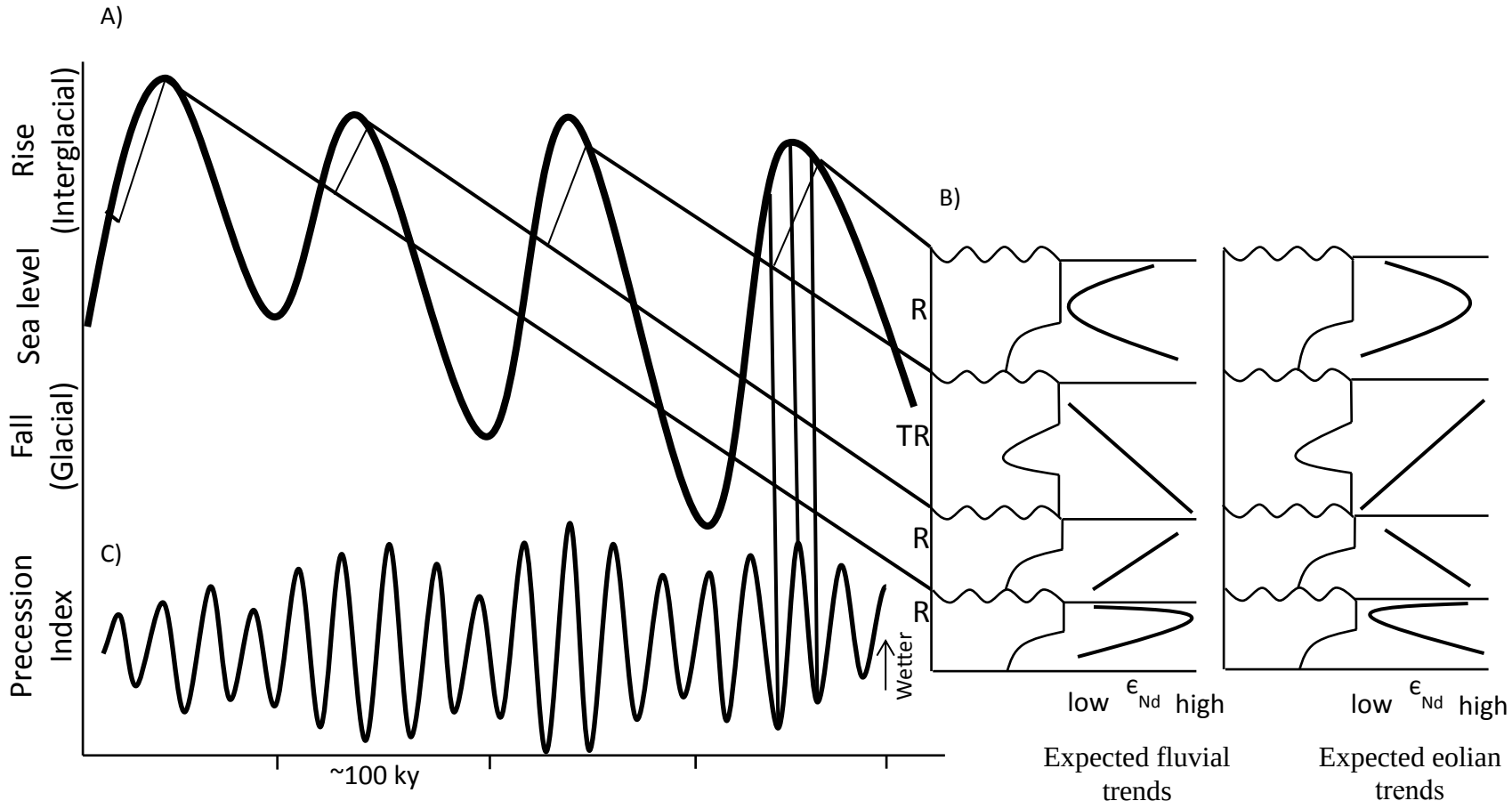
A)
Rise
(Interglacial)
Sea level
Fall
(Glacial)
Precession
Index
C)
~100 ky
Wetter
B)
R
TR
R
R
low ϵNd high
low ϵNd high
Expected fluvial trends
Expected eolian trends

Figure 6- Simplified diagram showing how cycles and corresponding ϵ_{Nd} trends are produced. A) Simplified sea-level curve generated by assumed eccentricity scale waxing and waning of large continental glaciers. The downward sloping black line is representing a certain subsidence rate, which remains constant over this relatively short time interval and the thinner, upward sloping lines show carbonate sedimentation rates. Note that carbonate deposition will only occur during times when sea-level rise is sufficient to submerge the studied area (above upward sloping line and below the sea-level curve) and that carbonate sedimentation initiates at varying times after being submerged (lag time; see text for discussion). B) Associated stratigraphic column is one that would be generated given the specified subsidence rate, lag time, carbonate sedimentation rates and changes in eustasy. It is important to note each cycle represents approximately 100 ky, but the majority of that time is represented by a disconformity (non-deposition) when subaerial exposure features develop. C) Simplified eccentricity modulated precession curve which shows variability in the amplitude of precessional changes controlled by the eccentricity of Earth's orbit where high eccentricity is associated with larger amplitude precessional changes. Note that high precession is associated with wetter low-latitude climates (see text discussion). Precession peaks are associated with wetter low-latitude climates, which increase CWF and shift ϵ_{Nd} values lower. Precession troughs are associated with relatively drier low-latitude climates, which decrease CWF and shift ϵ_{Nd} values higher. This ~10 ky variability (half of a precession cycle) is what causes shifts in ϵ_{Nd} values and, depending on when carbonate sedimentation occurs, can produce variable ϵ_{Nd} trends (recognized trends from this study are shown). Vertical lines in (B) are presented in the last cycle to more easily show how

ϵ_{Nd} trends could develop. The left vertical line is associated with the bottom part of the top cycle. The base of the cycle records drier conditions because carbonate sedimentation coincides with a precession trough. The middle of the carbonate cycle records wetter conditions because it coincides with a precession peak. The top of the carbonate cycle records drier conditions because sedimentation occurs during a precession trough. The two different columns illustrate the different ϵ_{Nd} trends generated if CWF were dominantly fluvial or eolian derived.

interglacial) shallow subtidal facies accumulated above previously exposed subtidal limestones. During the maximum rate of sea level rise (maximum rate of deglaciation), deep subtidal facies accumulated, followed by shallow subtidal deposition during sea-level highstand (peak interglacial) and early fall (initial glacial onset) when sedimentation rates outpaced accommodation gains. During the subsequent sea-level fall/lowstand (early to peak glaciation), subtidal limestones in these updip locations were subaerially exposed (Figures 5 and 6).

The sequence of events that generated regressive cycles is the same as those of transgressive-regressive cycles, however there was no sediment accumulation during late sea level rise (early interglacial) after previous exposure events (Read et al., 1986) and/or rapid sea-level rise rates which outpaced carbonate accumulation. Lag time refers to the time it takes for carbonate production to reach its full potential after/during transgressions and can range from hundreds to thousands of years (Read et al., 1986; Goldhammer et al., 1987). Lag times combined with rapid sea level rises produces deepening, however once carbonate production reaches its full potential (which easily outpaces even rapid sea level rise) shallowing will occur. Repetition of these processes generates regressive cycles which lack transgressive bases (Figures 5 and 6).

Nd-isotope results

ε_{Nd} values for all 3 locations range between -12.3 to -5.95 (Table 4; Figure 2). In Arizona ε_{Nd} values range from -12.15 to -7.51, whereas in Nevada ε_{Nd} values range between -12.3 to -5.95. These values are within the range reported from previous studies of Lower through Upper Pennsylvanian carbonates from New Mexico (Theiling et al.,

Table 4- $^{143}Nd/^{144}Nd$, apparent ε_{Nd} (value at present), Sm and Nd concentrations (ppm), ε_{Nd} (t=310 My), data for sampled intervals. t=310 My is assumed as an approximate age of deposition for both cycles sampled in both the Horquilla Ls and Bird Spring Fm., in order to determine ε_{Nd} at the time of deposition.

Location	Cycle #	Sample #	$^{143}Nd/^{144}Nd$	Apparent ε_{Nd}	Sm(ppm)	Nd(ppm)	ε_{Nd} @ 300 My	2σ error on ε_{Nd}
Arrow Canyon, NV	1	0	0.511971	-13.0	0.203	1.112	-9.60	0.15
		0.2	0.511906	-14.3	0.344	1.857	-10.93	0.15
		0.4	0.511882	-14.7	0.159	0.879	-11.30	0.21
		1.1	0.511949	-13.4	0.063	0.416	-9.29	0.32
		1.5	0.512033	-11.8	0.226	1.518	-7.59	0.43
	2	2.7	0.512064	-11.2	0.584	3.741	-7.15	0.16
		3	0.512056	-11.3	0.219	1.429	-7.24	0.21
		3.2	0.512036	-11.7	0.418	2.635	-7.75	0.13
		3.5	0.512059	-11.3	0.238	1.456	-7.43	0.22
		3.9	0.512029	-11.9	0.200	1.208	-8.08	0.21
		4.2	0.512011	-12.2	0.611	2.926	-9.45	0.14
	3	4.4	0.511934	-13.7	0.655	3.953	-9.93	0.15
		4.7	0.511963	-13.2	0.900	4.115	-10.62	0.14
		5.2	0.511954	-13.3	0.673	4.183	-9.41	0.05
		5.9	0.511952	-13.4	0.749	2.793	-12.03	0.17
	4	6.3	0.512020	-12.0	0.220	1.733	-7.31	0.09
		6.8	0.511960	-13.2	0.111	0.667	-9.45	0.24
		7.3	0.512002	-12.4	0.395	2.392	-8.59	0.41
		7.7	0.511980	-12.8	0.109	0.630	-9.22	0.23
		8	0.512039	-11.7	0.076	0.457	-7.91	0.30
		8.3	0.511959	-13.2	0.165	0.963	-9.57	0.26

5	8.7	0.512028	-11.9	0.134	0.795	-8.15	0.34
	9.5	0.512062	-11.2	0.119	0.724	-7.39	0.24
	10.1	0.512043	-11.6	0.125	0.759	-7.78	0.21
	10.3	0.512072	-11.0	0.131	0.799	-7.19	0.12
	10.7	0.512072	-11.0	0.185	1.143	-7.12	0.36
	11	0.512038	-11.7	0.153	0.927	-7.86	0.22
	11.3	0.512042	-11.6	0.426	2.643	-7.71	0.19
	11.7	0.512003	-12.4	0.431	2.665	-8.49	0.14
	12.1	0.511956	-13.3	0.549	3.158	-9.70	0.11
	12.5	0.511969	-13.0	0.326	1.915	-9.34	0.18
	12.9	0.511982	-12.8	0.324	1.871	-9.16	0.17
	13.4	0.511987	-12.7	0.246	1.384	-9.17	0.16
	14	0.512001	-12.4	0.288	1.611	-8.92	0.22
	14.5	0.511978	-12.9	0.133	0.840	-8.89	0.22
	14.8	0.511938	-13.7	0.106	0.705	-9.47	0.39
	15.2	0.512133	-9.9	0.236	1.456	-5.95	0.17
6	16.2	0.512113	-10.2	0.177	1.195	-6.02	0.27
	17.3	0.512062	-11.2	0.459	3.008	-7.11	0.15
	17.8	0.512120	-10.1	0.422	2.658	-6.13	0.15
	18.8	0.512113	-10.2	0.330	2.086	-6.25	0.16
	19.3	0.512115	-10.2	0.392	2.454	-6.24	0.18
	19.8	0.512125	-10.0	0.270	1.645	-6.16	0.16
	20.3	0.512008	-12.3	0.595	3.924	-8.15	0.17
	21.4	0.512029	-11.9	0.147	0.970	-7.73	0.23
	21.8	0.512032	-11.8	0.115	0.760	-7.66	0.39
	22.2	0.512073	-11.0	0.211	1.314	-7.09	0.29
7	23.5	0.512045	-11.6	0.127	0.720	-8.01	0.33
	23.9	0.512034	-11.8	0.135	0.770	-8.22	0.38
	24.5	0.512006	-12.3	0.240	1.441	-8.53	0.18
	25.6	0.512007	-12.3	0.179	1.013	-8.78	0.45
8	25.9	0.512086	-10.8	0.674	4.919	-6.26	0.20

Dry Canyon, AZ	1	2.3	0.512056	-11.3	0.120	0.722	-7.54	0.29
		2.6	0.512058	-11.3	0.201	1.126	-7.81	0.14
		3.4	0.512048	-11.5	0.313	1.902	-7.67	0.10
		3.9	0.511988	-12.7	0.173	0.946	-9.29	0.20
	2	4.5	0.511863	-15.1	0.397	2.284	-11.50	0.24
		4.8	0.511874	-14.9	0.411	2.301	-11.40	0.14
		5.2	0.511872	-14.9	0.585	3.336	-11.37	0.12
		5.9	0.511911	-14.2	0.266	1.511	-10.61	0.15
		6.6	0.511986	-12.7	0.285	1.496	-9.50	0.26
		7.1	0.512027	-11.9	0.209	1.177	-8.40	0.12
		7.7	0.511968	-13.1	0.156	0.870	-9.58	0.22
	3	8.2	0.511966	-13.1	0.156	0.829	-9.84	0.17
		10.2	0.511988	-12.7	0.596	3.621	-8.84	0.09
	4	12.2	0.511901	-14.4	0.448	2.497	-10.89	0.07
		13.7	0.511895	-14.5	0.514	2.783	-11.14	0.15
		14	0.511881	-14.8	0.183	0.987	-11.44	0.11
		14.6	0.511891	-14.6	0.269	1.437	-11.26	0.08
		15.5	0.511901	-14.4	0.187	0.997	-11.08	0.11
	5	20.5	0.511948	-13.5	0.406	2.186	-10.14	0.12
		21.3	0.511952	-13.4	0.334	1.816	-10.01	0.12
		22.2	0.511944	-13.5	0.242	1.328	-10.12	0.11
		22.9	0.511963	-13.2	0.098	0.507	-10.04	0.15
		23.1	0.511978	-12.9	0.060	0.313	-9.71	0.13
	6	24.3	0.512026	-11.9	0.367	2.247	-8.07	0.29
		24.7	0.512007	-12.3	0.063	0.366	-8.67	0.11
		25.1	0.511954	-13.3	0.300	1.775	-9.61	0.10
		25.6	0.511999	-12.5	0.180	1.066	-8.73	0.52
		26	0.512026	-11.9	0.129	0.787	-8.09	0.17
		26.5	0.512025	-12.0	0.153	0.924	-8.14	0.13

Gunnison Hills, AZ	1	0.4	0.511969	-13.1	0.308	1.692	-9.64	0.05
		2.1	0.511994	-12.6	0.537	2.956	-9.14	0.06
		2.4	0.512039	-11.7	0.213	1.137	-8.39	0.09
		3	0.512017	-12.1	0.195	0.963	-9.18	0.15
		3.3	0.511971	-13.0	0.177	1.051	-9.27	0.11
	2	3.5	0.511929	-13.8	0.751	4.123	-10.42	0.10
		4	0.512041	-11.6	0.542	3.564	-7.51	0.08
		4.4	0.511990	-12.6	0.706	3.779	-9.34	0.07
		4.8	0.511972	-13.0	0.333	1.883	-9.46	0.15
		5.3	0.511988	-12.7	0.424	2.401	-9.14	0.08
		5.6	0.511984	-12.7	0.424	2.222	-9.54	0.12
		6.1	0.512000	-12.5	0.752	4.417	-8.75	0.11
		6.5	0.511979	-12.9	0.302	1.760	-9.18	0.19
		8	0.511990	-12.6	0.331	1.811	-9.24	0.17
		9.5	0.511979	-12.8	0.221	1.133	-9.74	0.21
	3	10.2	0.511903	-14.3	0.388	2.146	-10.88	0.28
		11	0.511932	-13.8	0.145	0.754	-10.60	0.21
		11.2	0.511997	-12.5	0.077	0.376	-9.66	0.26
	4	11.5	0.511982	-12.8	0.155	0.928	-9.00	0.19
		12.7	0.512043	-11.6	0.224	1.305	-7.94	0.16
		13	0.512018	-12.1	0.236	1.347	-8.51	0.95
		13.5	0.512000	-12.4	0.246	1.427	-8.80	0.22
		14.3	0.511917	-14.1	0.609	3.258	-10.77	0.16
		15.2	0.511898	-14.4	0.234	1.132	-11.61	0.15
	5	16.5	0.511881	-14.8	0.665	3.615	-11.39	0.10
		17.1	0.512001	-12.4	0.854	4.982	-8.76	0.10
		18	0.512012	-12.2	0.763	4.358	-8.63	0.10
		18.7	0.512000	-12.4	0.753	4.426	-8.74	0.13
		19.5	0.511994	-12.6	0.733	4.227	-8.93	0.11
		20	0.511953	-13.4	2.867	14.991	-10.16	0.10
	6	20.5	0.511981	-12.8	0.467	2.651	-9.25	0.09

a.Value of εNd at present day.

b. εNd during estimated time of deposition (300 My), where 147Sm/144Nd=Sm(ppm)/ Nd(ppm)∗Natural abundance of 147Sm/144Nd∗atomic weight of Nd/Sm, then 143Nd/ 144Nd(t=310 My)=143Nd/144Ndmeasured−(eλt−1)∗ 147Sm/144Nd, and εNd(t=310 My)= (143Nd/144Nd(t=310 My)/143Nd/144NdCHUR(t=310 My)−1)∗10,000.

.

2012) Nevada, the US Midcontinent, Texas Midland basin, and southern Mexico (Woodard et al., 2013) (Figure 7).

Errors on individual ε_{Nd} values were determined using replicate analysis and range between 0.05 and 0.52 ε-units with an average of 0.18 ε-units (2σ) (Table 4; Figure 2). Error bars of less than 0.30 ε-units are smaller than the data points shown in Figure 2. The La Jolla Nd isotopic standard was run before and after each batch of samples, and a $^{143}Nd/^{144}Nd$ ratio of 0.511825±4 (2σ) was measured, which is within the accepted range of values for the standard (Pier et al., 1989).

Two repeating, high-frequency Nd-isotope trends are observed in Nevada and Arizona (Figure 2). Trend 1 is characterized by high ε_{Nd} values at the cycle base followed by a shift to lower values in the middle of the cycle and a return to higher values at/near cycle caps. A variation on this trend is that the higher values at the cycle base are missing (due to longer periods of non-deposition within a eustatic cycle) and the cycle begins with low ε_{Nd} values and shifts to higher values at the cycle top (Figure 2). In both trends, low ε_{Nd} values characterize what is interpreted to represent eustatic highstands or near highstands (interglacial stages) and overlying higher ε_{Nd} values occur during early sea-level fall (earliest glacial onset). Trend 1 occurs in 30% of cycles at Dry Canyon, Arizona, 20% of cycles at Gunnison Hills, Arizona, and <30% of cycles at Arrow Canyon, Nevada.

Trend 2 is the opposite of trend 1 and is characterized by low ε_{Nd} values at the cycle base followed by a shift to higher values in the middle of the cycle and a return to lower values at/near cycle caps. A similar variation on trend 2 is that the low ε_{Nd} values at the cycle base are missing (again due to longer periods of non-deposition within a

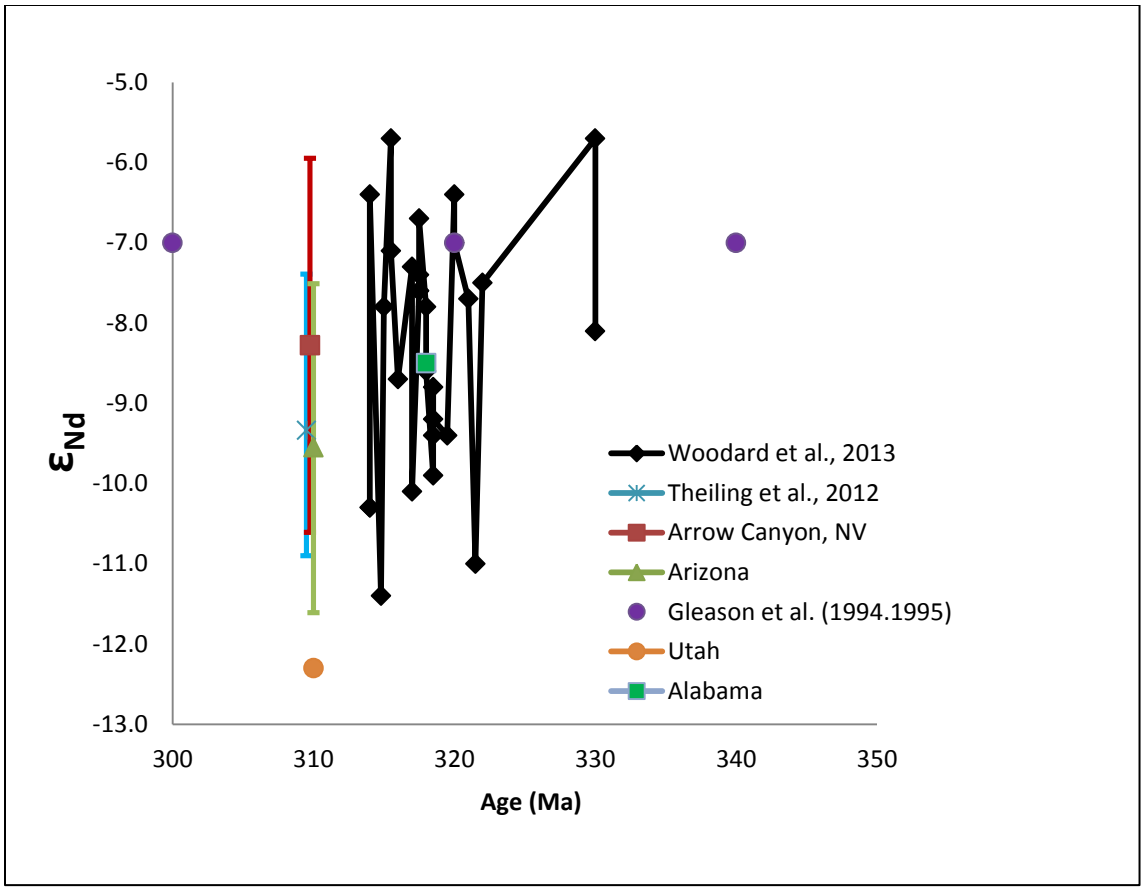

Figure 7- Various Carboniferous ε_{Nd} values. The black diamonds the black lines are values reported by Woodard et al. (2013). Purple dots represent values obtained by Gleason, et al. (1994, 1995). Utah and Alabama data come from Keto and Jacobsen (1988). ε_{Nd} also shown for Theiling et al. (2012) with bars representing the range of values reported. Red and green data are from this study with associated bars representing the range of values reported.

eustatic cycle) and the cycle begins with higher values and shifts to lower values towards the cycle top (Figure 2). In both trends, interpreted eustatic highstands (peak interglacials) or near highstands are characterized by higher ε_{Nd} values followed by decreasing values into the cycle cap (earliest glacial onset). Trend 2 is recorded in 15% of cycles at Dry Canyon, 80% of cycles at Gunnison Hills, and 60% of cycles at Arrow Canyon.

One cycle at Dry Canyon and one at Arrow Canyon record no systematic intracycle trends and two cycles at Dry Canyon were not exposed well enough to adequately identify isotopic trends (Figure 2).

Nd-isotope interpretations

To better understand the origins of the measured ε_{Nd} values, a simple two-component mixing model was developed using the procedure of Faure (1986) (Figure 8). End member seawater and river water Nd concentrations were taken from modern values reported by Banner (2004). Middle Pennsylvanian ε_{Nd} values were estimated using the values of Proterozoic basement rocks in the southern Ancestral Rockies reported by Bennett and DePaolo (1987) assuming the river waters draining into the Pedregosa basin reflect basement and overlying strata (and may include some amounts of eolian material blown into the drainage basins). Middle Pennsylvanian ε_{Nd} for the Panthalassa ocean are reported to be between -5 and -6 and were estimated using values obtained from open ocean carbonates accumulating on ophiolitic basement obducted onto southern Mexico (Woodard et al. 2013). . Values from these open marine carbonates may include some amount of eolian material blown directly from Pangea. The results from this simple

model suggest the measured ε_{Nd} values are dominated by input from Pennsylvanian seawaters rather than from fluvial/eolian input

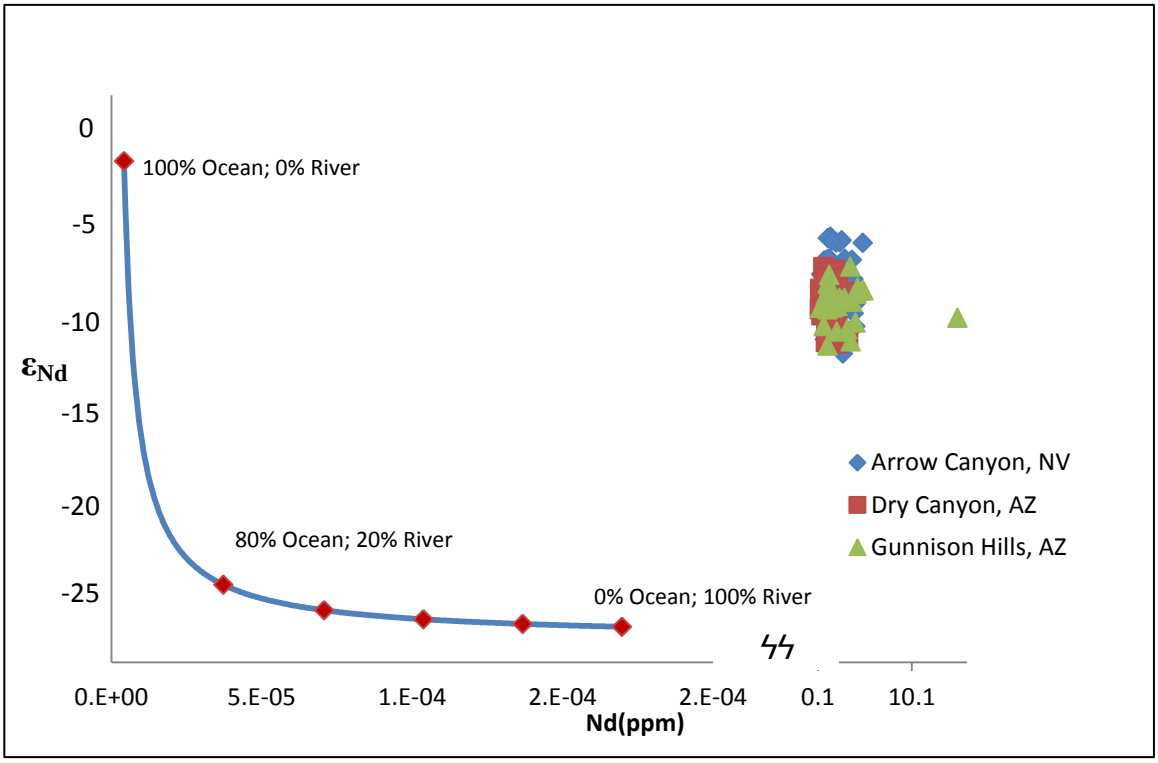

Figure 8- Two-component mixing line developed using the methodology of Faure (1986). Nd isotope concentrations are based on modern seawater and river water averages (Banner, 2004) and ε_{Nd} ratios for Precambrian basement and Panthalassa ocean come from Bennett and DePaulo (1987) and Woodard et al. (2013), respectively.

off the Ancestral Rocky Mountains (Figure 8). This is perplexing because based on our current understanding the marine Nd budget is dominated by fluvial input, however similar results were found by Burton and Vance (2000) who studied analyzed Nd-isotopes of planktic foraminifera in the Bay of Bengal next to one of the largest fluvial systems in the world, the Ganges-Brahmaputra. The Arrow Canyon, Nevada section has slightly higher average ε_{Nd} values than the other two Arizona sections likely because of its closer proximity to the Panthalassa ocean. The > 6 orders of magnitude higher Nd concentrations in the Pennsylvanian limestone samples versus estimated Pennsylvanian river water or seawater indicates extensive enrichment of Nd onto carbonate sediments which indicates extensive post-depositional enrichment of these epicontinental seaway limestones (e.g., Goldberg, 1954; Burton and Vance, 2000; Siddall et al., 2008).

High-frequency ε_{Nd} variability observed in this study as well as previous studies of coeval deposits (Theiling et al., 2012; Burton and Vance, 2000; Woodard et al., 2012) infers that any study evaluating Nd isotope trends on $>10^5$ yr time scales should sample at sub meter-scale intervals to prevent aliasing.

The two different high-frequency ε_{Nd} trends observed in this study imply either high continental weathering flux (CWF; lower ε_{Nd} values) during interglacials or the opposite of low CWF during interglacials (higher ε_{Nd} values). Individual stratigraphic sections show a mix of both trends; however, most of the studied cycles (45%) record low CWF (high ε_{Nd} values) during interglacials. In contrast, Middle Pennsylvanian (Desmoinesisan) tropical high-frequency cycles in central New Mexico record high CWF (low ε_{Nd} values) during interglacials (Theiling et al., 2012).

Trend 1

For those cycles recording high CFW (low ε_{Nd} values) during interglacials, this could be explained by increased fluvial sediment/dissolved load input into the studied marine basins related to wetter regional continental climates (increased fluvial discharge and/or increased continental weathering rates due to greater precipitation rates), or warmer regional continental climates (increasing continental weathering rates). Alternatively, if the CWF was sourced dominantly from eolian input, then interglacials represent drier/winder climates in upwind eolian source areas or there was a shift in wind directions towards the study areas during interglacials.

Trend 2

For those cycles recording low CWF (high ε_{Nd} values) during interglacials (45%) this could be the result of decreased fluvial sediment/dissolved load input due to drier and/or cooler regional continental climates, decreased eolian influx related to wetter/less windy climatic conditions in upwind source areas, or a change in wind directions away from study areas. Alternatively, the decrease in fluvial input during interglacials (sea-level highstands) could simply be the result of shoreline transgression and a landward shift of continental sediment/dissolved load farther away from the marine study areas.

DISCUSSION

Wet versus dry interglacials?

Previous studies of Pennsylvanian, Permian, and Neogene paleotropical regions suggest that interglacials could be either wetter/warmer or drier/cooler/windier. Soreghan (1992) reports wetter interglacial stages from Upper Pennsylvanian-Permian cycles in the Pedregosa and Paradox basins using the abundance and stratigraphic distribution of eolian deposits. Rankey (1997) used subaerial exposure of subtidal

sediments, fluvial incision through subtidal sediments, and paleosol characteristics within Pennsylvanian – Permian cyclic deposits and concluded that interglacials were wetter and more seasonal. In contrast, Miller et al. (1996) interpret drier Early Permian (Wolfcampian) interglacials using the character of paleosols interbedded with cyclic marine deposits. Cecil et al. (2003) developed a model that suggests during glacial periods a high pressure zone developed over the ice cap which confined shifts in the ITCZ creating a permanent low pressure zone over the equator leading to wetter glacials. Burton and Vance (2000) interpret Nd-isotope trends from late Neogene marine cores from the Bay of Bengal as indicating wetter interglacials. Lastly, Rea (1994) examined the eolian dust signal from more than 50 ocean cores which show a decrease in eolian sediment during interglacials suggesting wetter interglacial climates. From these various examples, it is apparent that there is no clear consensus on paleotropical interglacial climatic conditions during a range of icehouse climates.

Recently Horten et al. (2012) addressed this apparent discrepancy of wetter vs. drier low-latitude climates during glacial-interglacial stages using GCM climate models and key parameters including high-latitude ice sheet dynamics, response of high-latitude plant ecosystems, orbital forcing (using 80 ky eccentricity for simplicity), and pCO_2 varying between 420 ppm and 840 ppm. Their modeling results suggest that atmospheric pCO2 exerts the primary control over low-latitude continental climates and high-latitude glaciation. Intervals of high eccentricity amplified precession-driven changes in insolation promoted lower continental ice volume (high sea levels) and ice-volume changes as well as increased low-latitude precipitation variability. Specifically, precipitation highs alternated with precipitation lows on ~10 ky time scales (see their

Figure 9). During low eccentricity, amplification of precession-driven insolation was diminished which resulted in more stable and larger continental ice volumes (low sea levels) and less variability in low-latitude precipitation.

Several studies have documented orbitally driven insolation changes enhance the latitudinal extent of intertropical convergence zone (ITCZ) shifts (Wang et al., 2004; Wang et al., 2008; Landais et al., 2009) and that these enhanced shifts can explain the origins of 10 ky-scale low-latitude precipitation fluctuations (Wang et al., 2004; Wang et al., 2008; Landais et al., 2009). Wang et al. (2008) examined oxygen isotopes in speleothems from China from the past 224 ky and found a remarkable correspondence with speleothem growth (wet periods) and peaks in insolation. Similarly, Landais, et al. (2009) report oxygen isotopes from ice core data for the past 800 ky and found that variations in $\delta^{18}O$ are related to monsoon intensity, where increased monsoon intensity matches insolation peaks and decreased monsoon intensity correspond to insolation lows. Combining these results with Horton et al. (2012) suggests that precession driven insolation changes influence the position of the ITCZ which in turn controls low-latitude precipitation variations.

The implications of these models and corresponding data are that during a single, complete eccentricity-scale glacio-eustastic cycle, low-latitude regions have the potential to experience approximately five wetter alternating with drier climate variations; these wet-dry climate alternations being the result of ~5 precession cycles (~20 ky) occurring during a single eccentricity (~100 ky) cycle. However in reality, along any carbonate platform with fluctuating subsidence, sedimentation rates, lag times, and variable sea-level magnitudes, the number and pattern of ~10 ky wetter vs drier climate alternations

within a single glacio-eustatic cycle will vary, mainly due to the extent of abbreviation of individual stratigraphic cycles (Figure 6).

Figure 6 illustrates a potential range of cycle types (TR vs R) and Nd-isotope trends (Trend 1 vs Trend 2) that could develop given the interplay of cyclostratigraphic drivers (subsidence, sedimentation, lag time, sea level) and climate drivers (eccentricity and precession-driven precipitation changes). Regressive cycle 1 records a symmetric ε_{Nd} trend because the onset of cycle accumulation coincides with a precession high (higher precipitation), is followed ~10 ky later by a precession low (lower precipitation), with the cycle cap developing during a precession high. If CWF were primarily eolian sourced, the ~10 ky-paced wet-dry alternations would generate an ε_{Nd} pattern of initial high ε_{Nd} (low CWF) associated with higher precipitation (wetter upwind source areas), followed by a shift to lower ε_{Nd} (high CWF) associated with lower precipitation (drier upwind source areas), and a return to high ε_{Nd} (low CWF) with higher precipitation rates (wetter upwind source areas).

On the other hand, if CWF were primarily fluvial sourced, the ~10 ky-paced wet-dry alternations would generate the opposite ε_{Nd} trends. The low ε_{Nd} values (high CWF) at the cycle base would be associated with higher precipitation rates followed by a shift to higher ε_{Nd} (low CWF) associated with lower precipitation, and a return to low ε_{Nd} (higher CWF) associated with higher precipitation. Regressive cycle 2 records an abbreviated ε_{Nd} trend 2 simply because the onset of cycle accumulation occurred later within the eustatic cycle only capturing one wet-dry alternation. If CWF were primarily eolian sourced the ~10 ky-paced wet-dry alternations would generate the pattern of initial high ε_{Nd} (low CWF) related to wetter upwind source areas, followed by a shift to lower ε_{Nd}

(high CWF) and drier upwind source areas. If CWF were primarily fluvial sourced the opposite ε_{Nd} trend would be generated. T-R cycle 3 develops in response to a shorter lag time (compared to cycles 1, 2 and 4) and an abbreviated ε_{Nd} trend is generated for similar reasons as cycle 2; cycle accumulation only occurs during one wet-dry alternation. If CWF was primarily eolian sourced the ε_{Nd} trend is initially low (high CWF) associated with lower precipitation (drier upwind source areas), followed by a shift to higher ε_{Nd} (low CWF) associated with higher precipitation (wetter upwind source areas). If CWF were primarily fluvial sourced the generated ε_{Nd} trend would be opposite. Regressive cycle 4 records a symmetric ε_{Nd} trend and forms similar to cycle 1. If CWF were primarily eolian sourced, the ~10 ky-paced wet-dry alternations would generate the ε_{Nd} pattern of initial low ε_{Nd} (high CWF) associated with lower precipitation (drier upwind source areas), followed by a shift to higher ε_{Nd} (low CWF) associated with higher precipitation (wetter upwind source areas), and a return to low ε_{Nd} (high CWF) with lower precipitation rates (drier upwind source areas). On the other hand if CWF were primarily fluvial sourced the opposite trend would be produced.

Additional complexities to the interplay between cyclostratigraphic and climate drivers are different range precession frequencies varying from ~19 ky to 23 ky superimposed with the range of eccentricity frequencies (~95-125 ky) which will shift the number and timing of precession cycles (or wet-dry alternations) occurring within an eccentricity-scale eustatic cycle.

The previous discussions illustrate how during interglacials stages 1) a single locality can record either high or low ε_{Nd} values (Arrow Canyon, Nevada and Dry Canyon, Arizona), 2) a single locality can record consistently high ε_{Nd} values (Gunnison

Hills, Arizona) or low ε_{Nd} values (Theiling et al., 2012), or 3) closely spaced sections within the same basin record opposing trends (Dry Canyon vs Gunnison Hills, Arizona).

Dust versus fluvial CWF?

Although Nd-isotope trends from this study show definitive evidence of glacial-interglacial scale variations in CWF, it is not readily apparent from these particular interglacial- or sea-level highstand-dominated cycles whether ε_{Nd} trends were controlled by eolian or fluvial influx. Without determining whether the CWF was eolian or fluvial sourced, definitive glacial-interglacial climatic interpretations from Nd isotope trends are not possible.

However, several lines of evidence suggest that the observed CWFs were dominated by eolian sources. At each of the three study areas, Desmoinesian deposits lack interbedded coarse sand through gravel size detrital deposits, channelized bed geometries, or erosional fluvial features typical of higher gradient fluvial systems which would developed in response to large magnitude sea-level oscillations (Heckel, 1986; Algeo and Heckel 2008). Also lacking are typical deltaic deposits typical of many Pennsylvanian cyclic succession (Ferm, 1970; Gleason et al., 2007). Instead, the <10% siliciclastics present in the studied Desmoinesian successions are dominated by clay-silt size grains within deeper subtidal argillaceous lime mudstones—these grain sizes lies within the typical size fraction of eolian deposits.

Previous stratigraphic studies of late Paleozoic successions throughout the western and Southwestern US argue convincingly for the accumulation of thick, widespread, and blanket-like loess deposits attesting to windy and arid tropical conditions throughout the Pennsylvanian and Early Permian (Soreghan, 1992; Cecil et al., 2003;

G.S.Soreghan et al., 2002a; M. Soreghan et al., 2002b; Soreghan et al., 2008a and 2008b). In addition, Rice and Loope (1991) report Pennsylvanian and Permian eolian carbonates accumulating in southern Nevada and northern Arizona attesting to dry windy conditions during the development of glacial-interglacial cycles.

Interpretations of eolian versus fluvial sources for the abundant fine siliciclastic deposits includes volumetric, geometric, mineralogic, geochemical, and timing evidence and suggests that the late Paleozoic tropics in the US Southwest were semi-arid and remarkably dust prone. These recent interpretations suggest that although fluvial-sourced CWF cannot be ruled out, an interpretation for eolian-sourced CWF for observed Nd-isotope trends is preferred. Additional studies to differentiate between eolian vs. fluvial CWF include detailed siliciclastic grain size and sorting analysis.

Conclusions

1) Two types of orbital-scale, glacio-eustatic subtidal cycles are documented including transgressive-regressive and regressive. Due to interpreted large magnitude sea-level changes and the position of study areas along the inner/middle platform, the cyclostratigraphic record is dominated by highstand (interglacial) deposition with many cycle caps showing evidence of subaerial exposure (desiccation cracks and infilling calcretes, rhizoliths, meteoric cements, and moldic porosity) developed during initial rising (initial deglaciation), falling (glacial onset), lowstand (glacial) sea-level positions.

2) Two ϵ_{Nd} trends are recognized. Trend 1 is characterized by low ϵ_{Nd} (high CWF) during sea-level highstands (interglacial stages) and the opposite of high ϵ_{Nd} (low CWF) during sea-level highstands (interglacial stages) These contrasting trends are recorded

within a single stratigraphic section, as well as between sections indicating temporal and spatial variability.

3) The absence of fluvial deposits within the Pedregosa (Arizona) and Bird Spring (Nevada) basins combined with previous reports of thick Pennsylvanian loess deposits throughout the U.S. Southwest (Soreghan, 1992; Soreghan et al., 2002a; Cecil et al., 2003; Soreghan et al. 2008) suggests an eolian source for the observed CWF. If eolian sourced CWF is correct and we utilize recent climate modeling results (Horton et al., 2012) of late Paleozoic low-latitude precipitation variability, then the opposing ϵ_{Nd} trends during interglacial stages (highstands) are better understood. High CWF (low ϵ_{Nd}) during interglacials (trend 1) represents drier/more windy climates in upwind source areas, whereas low CWF (high ϵ_{Nd}) during interglacials (trend 2) implies wetter/less windy climates in upwind source areas. These interpreted wetter vs drier interglacial climates were controlled by eccentricity- amplification of precession-driven changes insolation and associated low latitude precipitation (Horton et al., 2012).

REFERENCES

Algeo, T., Wilson, J.L., and Lohmann, K.C., 1991, Eustatic and tectonic controls on cyclic sediment accumulation patterns in Lower-Middle Pennsylvanian strata of the Orogrande Basin, New Mexico, New Mexico Geological Society Guidebook 42, 203–212.

Algeo, T. J., & Heckel, P. H. 2008, The Late Pennsylvanian midcontinent sea of North America: a review. Palaeogeography, Palaeoclimatology, Palaeoecology, 268(3), 205-221.

Anderson, R.Y., 1982, A long geoclimatic record from the Permian. Journal of Geophysical Research 87, 7285–7294.

Arsouze, T., Dutay, J.-C., Lacan, F., and Jeandel, C., 2007, Modeling the neodymium isotopic composition with a global ocean circulation model, Cemical Geology, 239, p. 165-177.

Arsouze T., Dutay J.-C., Lacan F. and Jeandel C. 2009, Reconstructing the Nd oceanic cycle using a coupled dynamical–biogeochemical model. Biogeosci. Discuss. 6, 5549–5588.

Asmerom, Y., 1999, Th–U fractionation and mantle structure. Earth and Planetary Science Letters 166, 163–175.

Aziz, H.A., Hilgen, F.J., van Luijk, G.M., Sluijs, A., Krause, M.J., Pares, J.M. and Gingerich, P.D., 2007, Astronomical climate control on paleosol stacking patterns in the upper Paleocene–lower Eocene Willwood Formation, Bighorn Basin, Wyoming, Geology, v. 36, p. 531-534.

Banner, J.L., 2004, Radiogenic isotopes: systematics and applications to earth surface processes and chemical stratigraphy, Earth-Science Reviews, v. 65, p. 141–194.

Bennett, V.C. and DePaolo, D.J., 1987, Proterozoic crustal history of the western U.S. as determined by Nd isotope mapping, GSA Bulletin, v. 99, p. 674-685.

Bishop, J. W., Montañez, I. P., Gulbranson, E. L., & Brenckle, P. L. 2009, The onset of mid-Carboniferous glacio-eustasy: Sedimentologic and diagenetic constraints, Arrow Canyon, Nevada. Palaeogeography, Palaeoclimatology, Palaeoecology, 276(1), 217-243.

Bishop, James W., Montanez, Isabel P., Osleger, David A., 2010, Dynamic Carboniferous climate change, Arrow Canyon, Nevada, Geosphere, v.6, p. 1-34

Blakey, R. http://jan.ucc.nau.edu/~rcb7/garm310.jpg

Burton, K. and Vance, D., 2000, Glacial-interglacial variations in the neodymium isotope composition of seawater in the Bay of Bengal recorded by planktonic foraminifera, Earth and Planetary Science Letters, v. 176, p. 425-441.

Busch, R. M., & Rollins, H. B. 1984, Correlation of Carboniferous strata using a hierarchy of transgressive-regressive units. Geology, v. 12 no. 8, p. 471-474.

Cassity, Paul E. and Langenheim, R.L. Jr., 1966, Pennsylvanian and Permian fusulinids of the Bird Springs Group from Arrow Canyon, Clark County, Nevada, Journal of Paleontology, v.40, p. 931-968.

Cecil, C. Blaine, Dulong, Frank T., West, Ronald R., Stamm, Robert, Wardlaw, Bruce and Edgar, N. Terence, 2003, Climate controls on the stratigraphy of a Middle Pennsylvanian cyclothem in North America, Society for Sedimentary Geology (SEPM), Special Publication no. 77, p. 151-180.

Cisne, J.L. 1986, Earthquakes recorded stratigraphically on carbonate platforms, Nature, v. 323, p. 320-322.

Connolly, W.M. and Stanton, R.J., 1992, Interbasinal cyclostratigraphic correlation of Milankovitch band transgressive-regressive cycles: Correlatio of Desmoinesian-Missourian strata between southeastern Arizona and the mid-continent of North America, Geology, v. 20, p. 999-1002.

Dickinson, W.R., 2006, Geotectonic evolution of the Great Basin: Geosphere, v. 2, p. 353–368.

Elrick, Maya and Read, Fred J., 1991, Cyclic ramp-to-basin carbonate deposits, Lower Mississippian, Wyoming and Montana: A combined field and computer modeling study, Journal of Sedimentary Petrology, v. 61, no. 7, p. 1194-1224.

Elrick, M. and Scott, L.A., 2010, Carbon and oxygen isotope evidence for high-frequency (104-105 yr) and My-scale glacio-eustasy in Middle Pennsylvanian cyclic carbonates, central New Mexico, Palaeogeography, Palaeoclimatology, Palaeoecology., v. 285, 307–320.

Eros, J. M., Montañez, I. P., Osleger, D. A., Davydov, V. I., Nemyrovska, T. I., Poletaev, V. I., & Zhykalyak, M. V. 2012, Sequence stratigraphy and onlap history of the Donets Basin, Ukraine: insight into Carboniferous icehouse dynamics. Palaeogeography, Palaeoclimatology, Palaeoecology, v. 313, p. 1-25.

Faure, G. 1986, Principles of isotope geology. John Wiley and Sons, Inc.

Ferm, J. C. 1970, Allegheny deltaic deposits. Deltaic sedimentation modern and ancient: Tulsa, Okla., Soc. Econ. Paleontologists and Mineralogists Spec. Pub, v. 15, p. 246-255.

Fischer, A. G., & Bottjer, D. J. 1991, Orbital forcing and sedimentary sequences. Journal of Sedimentary Research, v. 61, no. 7.

Gale, A.S., Hardenbol, J., Hathway, B., Kennedy, W.J., Young, J.R., and Phansalkar, V., 2002, Global correlation of Cenomanian (Upper Cretaceous) sequences: Evidence for Milankovitch control on sea level, Geology, v. 30, p. 291-294.

Gleason, J. D., Patchett, P. J., Dickinson, W. R., & Ruiz, J. 1994, Nd isotopes link Ouachita turbidites to Appalachian sources. Geology, v. 22, no. 4, p. 347-350.

Gleason, J. D., Patchett, P. J., Dickinson, W. R., & Ruiz, J. 1995, Nd isotopic constraints on sediment sources of the Ouachita-Marathon fold belt. Geological Society of America Bulletin, v. 107, no. 10, p. 1192-1210.

Gleason, J. D., Gehrels, G. E., Dickinson, W. R., Patchett, P. J., & Kring, D. A. 2007. Laurentian sources for detrital zircon grains in turbidite and deltaic sandstones of the Pennsylvanian Haymond Formation, Marathon assemblage, west Texas, USA. Journal of Sedimentary Research, v. 77, no. 11, p. 888-900.

Goldberg, E. D. 1954, Marine geochemistry 1. Chemical scavengers of the sea. The Journal of Geology, 249-265.

Goldhammer, R.K., Elmore, R.D., 1984, Paleosols capping regressive carbonate cycles in the Pennsylvanian Black Prince Limestone, Arizona. Journal of Sedimentary Petrology 54, 1124–1137.

Goldhammer, R.K., Dunn, P.A., Hardie, L.A., 1987, High-frequency glacioeustatic sealevel oscillations with Milankovitch characteristics recorded in Middle Triassic platform carbonates, American Journal of Science, v. 287, p. 853-892.

Goldstein, S. L., O'nions, R. K., & Hamilton, P. J. 1984, A Sm-Nd isotopic study of atmospheric dusts and particlates from major river systems. Earth and Planetary Science Letters, v. 70, no. 2, p. 221-236.

Goldstein, R. 1988, Paleosols of Late Pennsylvanian cyclic strata, New Mexico*. Sedimentology, v. 35, no. 5, p. 777-803.

Goldstein, R. H. 1991, Stable isotope signatures associated with palaeosols, Pennsylvanian Holder Formation, New Mexico. Sedimentology, v. 38, no. 1, p. 67-77.

Goldstein, S.J. and Jacobsen, S.B., 1987, The Nd and Sr isotopic systematic of river water dissolved material: Implications for the sources of Nd and Sr in seawater. Chem. Geol. (Isot. Geosci. Sect.), v.66, p.245-272.

Gradstein, F., and Ogg, J. 2004, Geologic time scale 2004–why, how, and where next!. Lethaia, v. 37, no. 2, p. 175-181.

Hardie, L. A., Bosellini, A., & Goldhammer, R. K. 1986, Repeated subaerial exposure of subtidal carbonate platforms, Triassic, northern Italy: evidence for high frequency sea level oscillations on a 104 year scale. Paleoceanography, vol. 1, no. 4, p. 447-457.

Heckel, P. H. 1986, Sea-level curve for Pennsylvanian eustatic marine transgressive-regressive depositional cycles along midcontinent outcrop belt, North America. Geology, v. 14, no. 4, p. 330-334.

Heckel, P.H., 1994, Evaluation of evidence for glacio-eustatic control over marine Pennsylvanian cyclothems in North America and consideration of possible tectonic effects. In: Dennison, J.M., Ettensohn, F.F. (Eds.), Tectonic and Eustatic Controls on Sedimentary Cycles: Tulsa, Oklahoma SEPM Concepts in Sedimentology and Paleontology, v. 4, pp. 65–87.

Horton, D. E., Poulsen, C. J., Montañez, I. P., & DiMichele, W. A. 2012, Eccentricity-paced late Paleozoic climate change. Palaeogeography, Palaeoclimatology, Palaeoecology, v. 331, p. 150-161.

Jeandel C., Bishop J. K. and Zindler A. 1995 Exchange of neodymium and its isotopes between seawater and small and large particles in the Sargasso Sea. Geochim. Cosmochim. Acta v. 59, p. 535–547.

Landais, A., Dreyfus, G., Capron, E., Masson-Delmotte, V., Sanchez-Goni, M.F., Desprat, S., Hoffman, G., Jouzel, J., Leuenberger, M., and Johnsen, S., 2010, What drives the millennial and orbital variations of $^{18}O_{atm}$? Quaternary Science Reviews, v. 29, p.235-246.

Joachimski, M.M., von Bitter, P.H., and Buggisch, W., 2006, Constraints on Pennsylvanian glacioeustatic sea-level changes using oxygen isotopes on conodont apatite. Geology v. 34, p. 277–280.

Johannesson K. H. and Burdige D. J. 2007, Balancing the global oceanic neodymium budget: Evaluating the role of groundwater. Earth Planet. Sci. Lett. v. 253, p. 129–142.

Johannesson, K. H., Chevis, D. A., Burdige, D. J., Cable, J. E., Martin, J. B., & Roy, M. 2011, Submarine groundwater discharge is an important net source of light and middle REEs to coastal waters of the Indian River Lagoon, Florida, USA. Geochimica et Cosmochimica Acta, v. 75, no. 3, p. 825-843.

Keto, L. S., & Jacobsen, S. B. 1988, Nd isotopic variations of Phanerozoic paleoceans. Earth and Planetary Science Letters, v. 90, no. 4, p. 395-410.

Kluth, C.F., and Coney, P.J., 1981, Plate tectonics of the Ancestral Rocky Mountains: Geology, v. 9, p. 10–15.

Kues, B.S. and Giles, K.A., 2004, The late Paleozoic ancestral Rocky Mountains system in New Mexico, in Mack, G.H., and Giles, K.A., eds., The Geology of New Mexico: A Geological History: New Mexico Geological Society Special Publication v. 11, p. 95-136.

Lacan F. and Jeandel C., 2005b, Neodymium isotopes as a new tool for quantifying exchange fluxes at the continent-ocean interface. Earth Planet. Sci. Lett. v. 232, p. 245–257

Laurin, J., Meyers, S.R., Sageman, B.B., Waltham, D., 2005, Phase-lagged amplitude modulation of hemipelagic cycles: a potential tool for recognition and analysis of sealevel change. Geology v. 33, p. 569–572.

Miller, K. B., McCahon, T. J., & West, R. R. 1996, Lower Permian (Wolfcampian) Paleosol-bearing cycles of the US Midcontinent; evidence of climatic cyclicity. Journal of Sedimentary Research, v. 66, no. 1, p. 71-84.

Olson, P.E., Kent, D.V., 1999, Long-period Milankovitch cycles from the Late Triassic and Early Jurassic of eastern North America and their implications for the calibration of the Early Mesozoic time-scale and the long-term behavior of the planets. Philosophical Transactions of the Royal Society of London v. 357, p. 1761–1786.

Olszewski, T. D., & Patzkowsky, M. E. 2003, From cyclothems to sequences: the record of eustasy and climate on an icehouse epeiric platform (Pennsylvanian-Permian, North American Midcontinent). Journal of Sedimentary Research, v. 73, no. 1, p. 15-30.

Piepgras, D.J. and Wasserburg, G.J., 1979, The isotopic composition of Nd in different ocean masses, Earth and Planetary Science Letters, v. 45, p. 223-236

Piepgras, D.J. and Wasserburg, G.J., 1980, Neodymium isotopic variations in seawater, Earth Planet. Sci. Letters, v. 50, p. 128-138.

Pier, J.G., Podosek, F.A., Luhr, J.A., Brannon, J.C., Ara-Gomez, J.J., 1989, Spinel–iherzolitebearing Quaternary volcanic centers in San Luis Potosi, Mexico, 2. Sr and Nd isotope systematics. Journal of Geophysical Research v. 94, p. 7941–7951.

Poulsen, C.J., Pollard, D., Montañez, I.P., Rowley, D., 2007, Late Paleozoic tropical climate response to Gondwanan deglaciation, Geology, v. 35, p. 771-774.

Rankey, E. C. 1997, Relations between relative changes in sea level and climate shifts: Pennsylvanian–Permian mixed carbonate-siliciclastic strata, western United States. Geological Society of America Bulletin, v. 109, no. 9, p. 1089-1100.

Rea, D.K., 1994, The paleoclimatic record provided by eolian deposition in the deep sea; the geologic history of wind. Reviews of Geophysics v. 32, p. 159–195.

Read, J. F., Grotzinger, J. P., Bova, J. A., & Koerschner, W. F. 1986, Models for generation of carbonate cycles. Geology, v. 14, no. 2, p. 107-110.

Ritter, S. M., Barrick, J. E., & Skinner, M. R. 2002, Conodont sequence biostratigraphy of the Hermosa Group (Pennsylvanian) at Honaker Trail, Paradox Basin, Utah. Journal Information, v. 76, no. 3.

Ross, C. A., & Sabins Jr, F. F. 1965, Early and Middle Pennsylvanian fusulinids from southeast Arizona. Journal of Paleontology, p. 173-209.

Rygel, M.C., Fielding, C.R., Frank, T.D., Birgenheier, L.P., 2008, The magnitude of Late Paleozoic glacioeustatic fluctuations: a synthesis. Journal of Sedimentary Research v. 78, p. 500–511.

Scott, L.A., Elrick, M., 2004, Cycle and sequence stratigraphy of Middle Pennsylvanian (Desmoinsian) strata of the Lucero Basin, central New Mexico. In: Lucas, S.G., Zeigler, K.E. (Eds.), New Mexico Museum of Natural History and Science Bulletin, pp. 31–41.

Siddall, M., Khatiwala, S., van de Flierdt, T., Jones, K., Goldstein, S. L., Hemming, S., & Anderson, R. F. 2008, Towards explaining the Nd paradox using reversible scavenging in an ocean general circulation model. Earth and Planetary Science Letters, v. 274, no. 3, p. 448-461.

Soreghan, G.S., Giles, K.A., 1999, Amplitudes of Late Pennsylvanian glacioeustasy. Geology v. 27, p. 255–258.

Soreghan, G. S. 1992, Preservation and paleoclimatic significance of eolian dust in the Ancestral Rocky Mountains province. Geology, v. 20 no. 12, p. 1111-1114.

Soreghan, G. L., Elmore, R. D., & Lewchuk, M. T. 2002a, Sedimentologic-magnetic record of western Pangean climate in upper Paleozoic loessite (lower Cutler beds, Utah). Geological Society of America Bulletin, v. 114, no. 8, p. 1019-1035.

Soreghan, M. J., Soreghan, G. L., & Hamilton, M. A. 2002b. Paleowinds inferred from detrital-zircon geochronology of upper Paleozoic loessite, western equatorial Pangea. Geology, v. 30, no. 8, p. 695-698.

Soreghan, G. S., Soreghan, M. J., & Hamilton, M. A. 2008a, Origin and significance of loess in late Paleozoic western Pangaea: a record of tropical cold?. Palaeogeography, Palaeoclimatology, Palaeoecology, v. 268, no. 3, p. 234-259.

Soreghan, M. J., Soreghan, G. S., & Hamilton, M. A. 2008b, Glacial–interglacial shifts in atmospheric circulation of western tropical Pangaea. Palaeogeography, Palaeoclimatology, Palaeoecology, v. 268, no. 3, p. 260-272.

Spooner, E. T. C. 1976, The strontium isotopic composition of seawater, and seawater-oceanic crust interaction. Earth and Planetary Science Letters, v. 31, no. 1, p. 167-174.

Strasser, A. 1984, Black-pebble occurrence and genesis in Holocene carbonate sediments (Florida Keys, Bahamas, and Tunisia). Journal of Sedimentary Research, v. 54, no. 4, p. 1097-1109.

Tachikawa, K., Jeandel, C. and M. Roy-Barman, 1999, A new approach to the Nd residence time in the ocean: The role of atmospheric inputs, Earth Planet. Sci. Lett., v.170, p. 433-446.

Theiling, Bethany P., Elrick, Maya, and Asmerom, Yemane, 2012, Increased continental weathering flux during orbital-scale sea-level highstands: Evidence from Nd and O isotope trends in Middle Pennsylvanian cyclic carbonates, Palaeogeography, Palaeoclimatology, Palaeoecology, v. 342-343, p. 17-26.

Veevers, J.M. and Powell, C. McA, 1987, Late Paleozoic glacial episodes in Gondwanaland reflected in transgressive–regressive depositional sequences in Euramerica. Geological Society of America Bulletin v. 98, p. 475–487

Wang, Xianfeng, Auler, Augusto S., Edwards, R. Lawrence, Cheng, Hai, Cristalli, Patricia S., Smart, Peter L., Richards, David A. and Chen, Chuan-Chou., 2004, Wet periods in noreastern Brazil over the past 210 kyr linked to distant climate anomalies, Nature, v. 432, p. 740-743.

Wang, Yongjin, Cheng, Hai, Edwards, R. Lawrence, Kong, Xinggong, Shao, Xiaohua, Chen, Shitao, Wu, Jiangyin, Jiang, Xiouyang, Wang, Xianfeng, and An, Zhisheng., 2008, Millennial-and orbital-scale changes in the East Asian Monsoon over the past 224,000 years, Nature, v. 451, p 1090-1093.

Wanless, H.R. and Cannon, J.R., 1966, Late Paleozoic glaciations, Earth-Science Reviews, v. 1, p. 247-286.

Wanless H.R. and Shepard, F.P., 1936, Sea level and climatic changes related to late Paleozoic cycles, Geological Society of America Bulletin, v. 47, p. 1177-1206.

Wilson, J. L. 1975. Carbonate Facies in Geologic History Springer. New York, 471.

Woodard, S.C., Thomas, D.J., Grossman, E.L., Olszewski, T.D.,Yancey, T.E., Miller, B.V., Raymond, A, 2013, Radiogenic isotope composition of Carboniferous seawater from North American epicontinental seas, Palaeogeography, Palaeoclimatology, Palaeoecology, v. 370, p. 51-63.